

## RESEARCH ARTICLE

## SPECIAL ISSUE: CELL BIOLOGY OF LIPIDS

# Characterization of lipoprotein lipase storage vesicles in 3T3-L1 adipocytes

Benjamin S. Roberts, Chelsea Q. Yang and Saskia B. Neher\*

## ABSTRACT

Lipoprotein lipase (LPL) is a secreted triglyceride lipase involved in the clearance of very-low-density lipoproteins and chylomicrons from circulation. LPL is expressed primarily in adipose and muscle tissues and transported to the capillary lumen. LPL secretion is regulated by insulin in adipose tissue; however, few studies have examined the regulatory and trafficking steps involved in secretion. Here, we describe the intracellular localization and insulin-dependent trafficking of LPL in 3T3-L1 adipocytes. We compared LPL trafficking to the better characterized trafficking pathways taken by leptin and GLUT4 (also known as SLC2A4). We show that the LPL trafficking pathway shares some characteristics of these other pathways, but that LPL subcellular localization and trafficking are distinct from those of GLUT4 and leptin. LPL secretion occurs slowly in response to insulin and rapidly in response to the Ca<sup>2+</sup> ionophore ionomycin. This regulated trafficking is dependent on Golgi protein kinase D and the ADP-ribosylation factor GTPase ARF1. Together, these data give support to a new trafficking pathway for soluble cargo that is active in adipocytes.

This article has an associated First Person interview with the first author of the paper.

**KEY WORDS:** Lipase, Triglyceride, ARF1 GTPase, Protein kinase D, Trafficking, Insulin

## INTRODUCTION

The secreted enzyme lipoprotein lipase (LPL) is essential for the clearance of post-prandial triglycerides (TGs) from the blood. Following a meal, TGs are packaged into lipoprotein particles and circulated through the bloodstream. LPL hydrolyzes the TGs packaged into chylomicrons and very-low-density lipoprotein particles, and participates in the uptake of remnant lipoprotein particles (Hayne et al., 2017). In the fed state, elevated adipose LPL activity enhances plasma TG clearance, in part through insulin signaling (Saltiel and Kahn, 2001). In type 2 diabetes (T2D) patients, poor insulin sensitivity is associated with low plasma LPL activity (Huang et al., 2013), and reduced LPL activity is associated with the development of cardiovascular disease, a major comorbidity in T2D (Saltiel and Kahn, 2001).

LPL is primarily expressed in muscle and adipose tissues (Semenkovich et al., 1989b). In adipose cells, *LPL* mRNA levels fluctuate throughout the day in response to feeding and fasting (Kroupa et al., 2012). In muscle and adipose, LPL transcription is

tightly regulated by the peroxisome proliferator-activated receptor (PPAR) family of transcription factors (Schoonjans et al., 1996; Ruby et al., 2010). In muscle, the intracellular energy sensor adenosine monophosphate kinase (AMPK) regulates mRNA levels, whereas other factors contribute to LPL biosynthesis in adipose tissue (An et al., 2005; Kim et al., 2007). Although much is known about the regulation of LPL biosynthesis (Li et al., 2002; Roberts et al., 2018), less is known about the role of insulin in packaging and trafficking mature LPL protein.


In adipocytes, insulin stimulation enhances LPL activity independent of biosynthesis (Semenkovich et al., 1989). For this reason, insulin-stimulated trafficking schemes used by other proteins provide useful models for studying insulin-stimulated LPL trafficking. The insulin-dependent post-translational regulation of glucose transporter 4 (GLUT4; also known as SLC2A4) is perhaps the best understood model of insulin-dependent protein trafficking. Following a meal, elevated plasma insulin levels trigger trafficking of GLUT4 to the plasma membrane (PM) to enhance glucose uptake (James et al., 1988) without affecting GLUT4 biosynthesis (Flores-Riveros et al., 1993). In adipocytes, GLUT4 is trafficked in specialized GLUT4 storage vesicles (GSVs) marked with clathrin, various RAB GTPases and insulin-sensitive transmembrane proteins (Jedrychowski et al., 2010). Like GLUT4, recent studies have also examined the trafficking of the soluble adipokine leptin in adipocytes. In addition to GLUT4, leptin secretion may be a useful model of insulin-stimulated protein trafficking. Leptin is trafficked in vesicles distinct from GSVs, and leptin secretion requires an insulin-dependent biosynthetic step (Wang et al., 2014). Thus, leptin is an alternative model cargo for studying regulated protein trafficking in adipocytes.

Early studies concluded that LPL must be maintained in an inactive, cryptic storage form in adipocytes (Pradines-Figueres et al., 1990). In this cryptic state, lysate LPL activity is concentration dependent (Pradines-Figueres et al., 1990), and both medium and lysate LPL activity are sensitive to insulin stimulation (Semenkovich et al., 1989). These findings could be attributed to regulated LPL trafficking. Later studies showed that brefeldin A (BFA) blocked LPL secretion and produced tubular LPL-marked vesicles without affecting intracellular LPL activity (Park et al., 1996). These findings hint at the existence of regulated LPL vesicles or lipase storage vesicles (LSVs) in adipocytes.

More recently, studies have shed light on the composition and possible regulation of LPL in LSVs. One study showed that the VPS-family proteins SorLA and sortilin mediate LPL degradation, but not LPL exocytosis (Klinger et al., 2011). In cardiomyocytes, LPL secretion is dependent on protein kinase D (PRKD) family proteins in an insulin-independent system (Kim et al., 2008). Another recent study showed that LPL exocytosis is dependent on the heparin sulfate proteoglycan (HSPG) syndecan 1 (SDC1) in HeLa cells. In these cells, LPL is trafficked in a regulated pathway, anchored by SDC1 and sorted into sphingomyelin (SM)-rich *trans*-Golgi membranes (Deng et al., 2018; Sundberg et al., 2019).

Department of Biochemistry and Biophysics, University of North Carolina at Chapel Hill, Chapel Hill, NC 27599, USA.

\*Author for correspondence (neher@med.unc.edu)

 B.S.R., 0000-0002-6450-2021; S.B.N., 0000-0003-4165-6674

Handling Editor: James Olzmann

Received 1 April 2021; Accepted 10 July 2021

In 3T3 cells, LPL is sequestered prior to insulin-stimulated secretion in SDC1-marked storage compartments (Gunn et al., 2020) which may represent LSVs.

Adipocytes shed SDC1 in response to insulin stimulation, which plays some role in the extracellular release of LPL from the cell surface (Reizes et al., 2006). Here, we present the first detailed molecular description of regulated intracellular LPL trafficking in a physiologically relevant system. We show that LPL colocalizes poorly with GLUT4 in adipocytes, and that their trafficking follows physically and kinetically distinct pathways in response to insulin. We find that an insulin-dependent biosynthetic step is required for LPL release, and that  $\text{Ca}^{2+}$  can bypass the need for insulin in stimulated secretion. Lastly, we show that Golgi PRKDs and ARF GTPases are required for LSV trafficking to the plasma membrane. These findings highlight the importance of insulin in regulated LPL secretion, and add to a growing body of research that describes atypical protein trafficking mechanisms.

## RESULTS

### Molecular characterization of LPL storage vesicles

We initially set out to describe the steady-state localization of LSVs in 3T3 adipocytes. We hypothesized that insulin stimulation would affect the colocalization of LPL with markers of other insulin-dependent trafficking pathways. We modeled our approach on studies of GLUT4 trafficking and began by staining fixed adipocytes for endogenous LPL and GLUT4. We found that LPL and GLUT4 appeared to be distributed differently under both conditions, and that the colocalization of LPL with GLUT4 did not differ between unstimulated ( $31\pm 20\%$ ; mean $\pm$ s.d.) and insulin-stimulated conditions ( $37\pm 16\%$ ) (Fig. 1A,I, quantified in Q). These data agreed with another study using different methodologies suggesting that most LPL and GLUT4 traffic separately (Roh et al., 2001).

Next, we turned our attention to basic vesicle markers associated with GSVs. GSVs are generally considered clathrin-coated vesicles (Camus et al., 2020), and do not usually localize to cholesterol-rich lipid microdomains marked by caveolin at the PM (Lizunov et al., 2013; Gao et al., 2017; Stenkula et al., 2010). Thus, we compared the colocalization of LPL with the membrane domain markers caveolin-1 (Cav1) and clathrin. We observed that a large amount of LPL colocalized with Cav1 under basal ( $70\pm 15\%$ ) and insulin-stimulated conditions ( $65\pm 14\%$ ) (Fig. 1C,K, quantified in Q). In addition to cholesterol, Cav1 associates with membrane domains enriched in SM (Caselli et al., 2002), in agreement with other findings that LPL is sorted into SDC1-marked SM-rich compartments (Sundberg et al., 2019). By contrast, less LPL colocalized with clathrin than Cav1 in both unstimulated ( $32\pm 14\%$ ) and insulin-stimulated ( $20\pm 13\%$ ) cells (Fig. 1B,J, quantified in Q). Furthermore, significantly less LPL colocalized with clathrin after insulin stimulation (Fig. 1Q). These results indicate that LPL primarily follows a Cav1-dependent trafficking pathway, but that some LPL could follow a clathrin-dependent pathway in unstimulated cells.

We next examined the colocalization of LPL with several Golgi markers. First, we analyzed the colocalization of LPL with the GLUT4-associated marker syntaxin 6 (STX6), a marker of GSVs trafficking bi-directionally between the *trans*-Golgi network (TGN) and endosomal network (Kumudu et al., 2003). We found that little LPL colocalized with STX6 in both unstimulated ( $16\pm 10\%$ ) and insulin-stimulated cells ( $18\pm 11\%$ ) (Fig. 1D,L, quantified in Q). This finding indicates that LPL could follow a different TGN trafficking pathway.

Because LPL colocalized poorly with STX6, we examined the colocalization of LPL with the TGN markers golgin-97 (also known

as GOLGA1) and the ADP-ribosylation factor-binding protein GGA2. Golgin-97 is a marker of a subset of post-Golgi cargo such as the matrix metalloproteases (MMPs) MMP2 and MMP7 (Eiseler et al., 2016) and GGA2 marks tubular TGN-to-endosome structures (Tie et al., 2018). We found that LPL colocalized with golgin-97 to a similar extent in unstimulated ( $46\pm 15\%$ ) and insulin-stimulated ( $39\pm 20\%$ ) cells (Fig. 1E,M, quantified in Q). Similarly, LPL colocalized with GGA2 to the same extent in unstimulated ( $49\pm 17\%$ ) and insulin-stimulated ( $48\pm 18\%$ ) cells (Fig. 1F,N, quantified in Q). Together, our data suggests that LPL is trafficked from a subset of TGN structures marked primarily with GGA2 and golgin-97 and undergoes some exchange between the TGN and endosomes.

In adipocytes, GLUT4 is sorted between the TGN and endosomes (Kumudu et al., 2003) which led us to examine the colocalization of LPL with several endosomal sorting markers. We found that some LPL colocalized with the early endosome marker EEA1 under unstimulated ( $40\pm 20\%$ ) and insulin-stimulated ( $38\pm 21\%$ ) conditions (Fig. 1G,O, quantified in Q). In addition to EEA1, we analyzed the colocalization of LPL with the GLUT4-associated markers RAB10 (Sano et al., 2007), LAMP1 (Xie et al., 2016), RAB4A (Imamura et al., 2003) and ARF6 (Yang and Mueckler, 1999). LPL colocalized with RAB10 to similar extents in unstimulated ( $51\pm 14\%$ ) and insulin-stimulated ( $44\pm 15\%$ ) cells (Fig. 1H,P, quantified in Q), indicating that LPL is partially localized to the late endosomes. LPL also colocalized with the fast-recycling endosome marker RAB4A in unstimulated ( $42\pm 14\%$ ) and insulin-stimulated ( $43\pm 11\%$ ) cells (Fig. S1A,D, quantified in G). Like GLUT4, LPL is targeted to lysosomes during degradation (Xie et al., 2016; Klinger et al., 2011). LPL colocalized with LAMP1 to equal extents in unstimulated ( $35\pm 11\%$ ) and insulin-stimulated cells ( $37\pm 11\%$ ) (Fig. S1B,E, quantified in G). Finally, we found that some LPL colocalized with the membrane marker ARF6 in unstimulated ( $39\pm 14\%$ ) and insulin-stimulated ( $43\pm 13\%$ ) cells (Fig. S1C,F, quantified in G).

Together, these data indicate that at steady-state LPL colocalizes with caveolar membranes in the TGN and endosomes. Furthermore, we conclude that LSVs follow a prescribed trafficking route that varies little between unstimulated and insulin-stimulated conditions. We proceeded to characterize other differences in unstimulated and insulin-stimulated LPL trafficking.

In addition to microscopy, subcellular fractionation has been used to characterize intracellular GLUT4 trafficking. Non-cycling GSVs are enriched in the large microsome fractions under basal conditions and in the small microsome fractions during insulin stimulation, with the large microsome fractions containing the Golgi, ER and PM, and the small microsome fractions containing mostly endosomes, GSVs and other small structures (Kupriyanova et al., 2002; Roh et al., 2001; Yeh et al., 2007). Because an earlier study showed that LPL does not cofractionate with GLUT4 under basal conditions (Roh et al., 2001), we asked whether insulin stimulation affected LPL trafficking relative to GLUT4 trafficking. We used a velocity fractionation approach to separate cellular components by size. Under basal conditions, both full-length ( $\sim 55$  kDa) and cleaved LPL ( $\sim 35$  kDa) LPL were enriched in large microsomes at the bottom of the gradient and were absent from the small microsomes entirely. GLUT4 was present in the small and large microsomes, partially overlapping with LPL (Fig. 2A). Whereas 30 min of insulin stimulation led to GLUT4 accumulation in small microsomes, LPL remained concentrated in the heaviest fractions (Fig. 2A). After 2 h of insulin stimulation, the remaining GLUT4 had returned to the large microsomal fractions due to endolysosomal

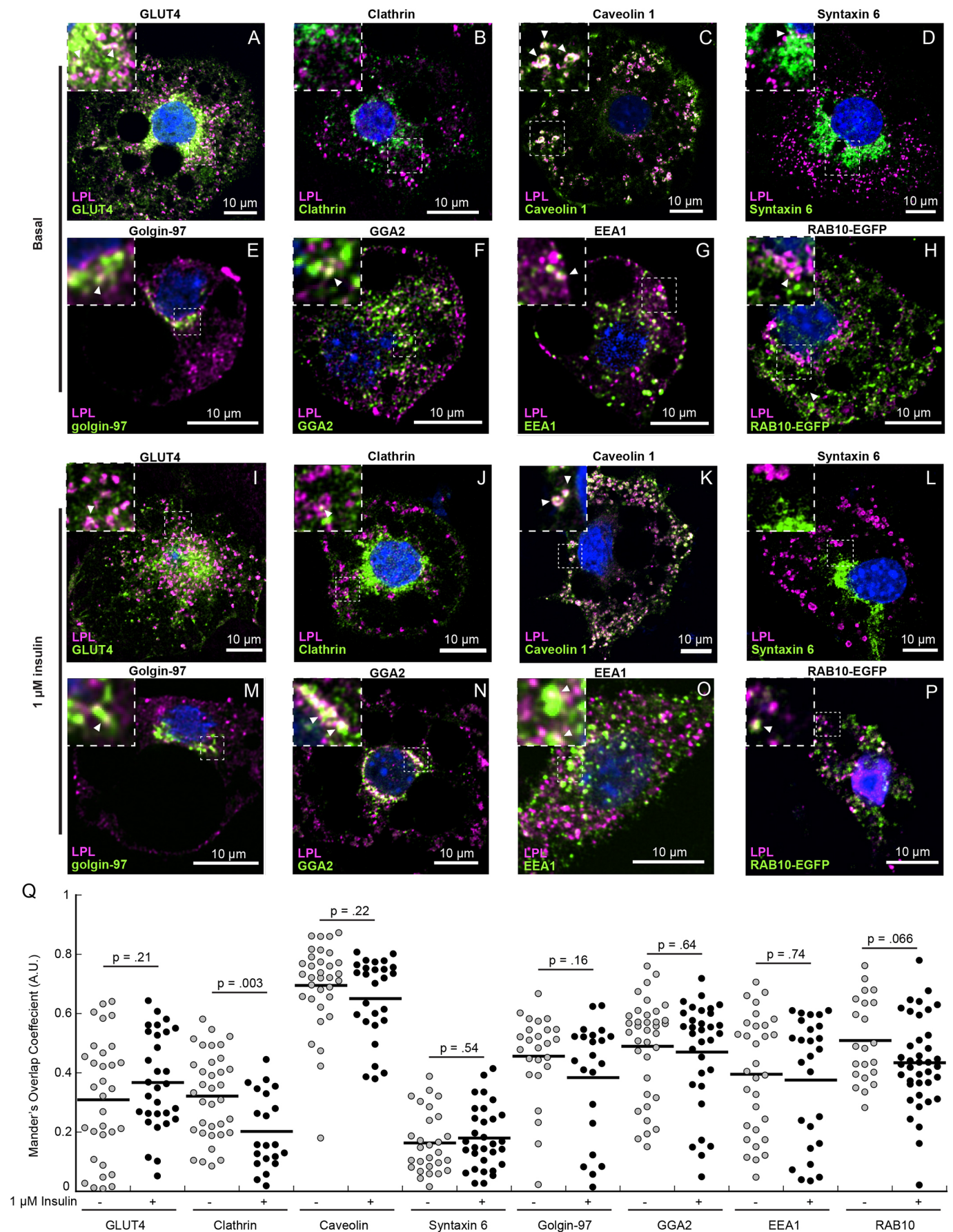


Fig. 1. See next page for legend.

**Fig. 1. Intracellular localization of LPL in 3T3-L1 adipocytes.** (A–H) Adipocytes were treated with vehicle (basal) or (I–P) with insulin for 120 min before being fixed and stained for the indicated target. Insets show selected magnified views of the indicated area. Examples of colocalizing puncta are indicated with arrowheads. Scale bars: 10  $\mu\text{m}$ . (Q) The colocalization of LPL with the indicated markers as indicated by the Mander's coefficient is shown (A.U., arbitrary units). All datasets are from three biological replicate sets: GLUT4 (basal  $n=32$ ; insulin-stimulated  $n=30$ ), clathrin (basal  $n=35$ ; insulin-stimulated  $n=21$ ), caveolin 1 (basal  $n=33$ ; insulin-stimulated  $n=27$ ), syntaxin 6 (basal  $n=28$ ; insulin-stimulated  $n=31$ ), golgin-97 (basal  $n=25$ ; insulin-stimulated  $n=22$ ), GGA2 (basal  $n=36$ ; insulin-stimulated  $n=32$ ), EEA1 (basal  $n=31$ ; insulin-stimulated  $n=26$ ), RAB10 (basal  $n=21$ ; insulin-stimulated  $n=29$ ). Each point reflects data from a single cell. *P*-values were calculated with a Student's *t*-test.

recycling, which is responsible for GLUT4 turnover in insulin-stimulated cells (Brewer et al., 2014; Xie et al., 2016). At this time point, LPL remained unmoved from large microsomal fractions, with a slight decrease in mass attributable to secretion of LPL into the medium (Semenkovich et al., 1989).

Together, these data indicate that, unlike GLUT4, which is exchanged between membranes during trafficking, LPL is trafficked in stable vesicles that undergo little change during insulin-stimulated trafficking. Instead, LPL vesicles may be Golgi or post-Golgi structures resembling caveolar SM microdomains. Our findings shown in Figs 1 and 2 suggest that unlike GSVs, LSVs could traffic directly between the Golgi and the PM.

After seeing the clear differences between GLUT4 and LPL trafficking, we turned our attention to an alternative model of cargo trafficking in adipocytes. The adipokine leptin is a soluble cargo secreted in response to extended insulin stimulation that does not cofractionate with GSVs (Wang et al., 2014). Thus, we examined the colocalization of LPL with leptin. We found that leptin was distributed in post-Golgi structures resembling LSVs and that 30–40% of LPL colocalized with leptin in unstimulated ( $40\pm 16\%$ ; mean $\pm$ s.d.) and insulin-stimulated ( $37\pm 20\%$ ) cells (Fig. 3A). This colocalization level was similar to the colocalization of LPL with GLUT4 (Fig. 1Q) and agreed with data from Roh et al. (2001) who showed that leptin, GLUT4 and LPL traffic separately in adipocytes. Different effectors regulate leptin vesicles and GSVs (Fig. 3B). Despite these differences, the morphological resemblance between LSVs and leptin vesicles was compelling. We hypothesized that LPL trafficking could more closely resemble leptin trafficking than GLUT4 trafficking, so we investigated the effects of known leptin effectors on LPL trafficking.

### The effect of insulin on LPL secretion

Insulin-stimulated leptin secretion takes several hours and involves a biosynthetic step (Wang et al., 2014). Contradictory studies have indicated that insulin plays either a transcriptional (Ong et al., 1988) or post-translational role (Vannier et al., 1989) in LPL trafficking, so we asked whether insulin-stimulated LPL secretion involved changes in LPL biosynthesis. To do so, we first analyzed the rate of LPL secretion to the medium in response to insulin stimulation. Like leptin, we found that LPL secretion takes place within 2 h of insulin treatment (Fig. 4A,B). For this reason, we conducted the remainder of our experiments after 120 min of vehicle or insulin treatment.

Whereas the ribosome inhibitor cycloheximide (CHX) inhibits insulin-stimulated leptin secretion (Wang et al., 2014), GLUT4 translocation is insensitive to CHX treatment (Slot et al., 1997). Thus, we treated cells with CHX prior to and during insulin stimulation and measured LPL in cell lysate and medium. We found

that, like leptin, both unstimulated and insulin-stimulated LPL secretion was sensitive to CHX treatment (Fig. 4C,D). Interestingly, CHX reduced LPL secretion to a consistently low level independently of insulin stimulation. This finding supports a trafficking model where bulk flow continuously releases a small amount of LPL into the medium, whereas CHX blocks an active regulated export pathway. To rule out the effect of LPL transcription in insulin-stimulated secretion, we measured levels of *LPL* mRNA using reverse-transcription real-time quantitative PCR (RT-qPCR) and found that insulin did not significantly alter LPL mRNA levels relative to GAPDH (Fig. S2).

Several prior studies have analyzed the effect of insulin on gene expression and protein biosynthesis. These studies have identified plausible insulin-regulated LPL partner proteins (Wang et al., 2004, 2006). We asked whether insulin affected the biosynthesis of one candidate, the LPL partner SDC1. However, we found that acute insulin stimulation did not significantly affect SDC1 protein levels (Fig. S3). Together, these findings show that insulin is not involved in either LPL or SDC1 biosynthesis in mature adipocytes. Instead, they show that acute insulin stimulation may regulate the biosynthesis of an unidentified protein required for regulated insulin-stimulated LPL secretion.

### Ca<sup>2+</sup> dependence of LPL secretion

Ca<sup>2+</sup> is essential in insulin signaling (Worrall and Olefsky, 2002) and both GLUT4 trafficking (Li et al., 2014) and leptin secretion (Wang et al., 2014) are sensitive to intracellular Ca<sup>2+</sup> levels. Thus, we first asked whether ionomycin was able to induce LPL secretion in the absence of insulin. To our surprise, ionomycin stimulated full-length LPL secretion in as little as 30 min, more quickly than insulin did (Fig. 5A). In contrast, we found that ionomycin treatment did not significantly enhance the secretion of the soluble protein adiponectin (Fig. S4). Together, these data indicate that high intracellular Ca<sup>2+</sup> levels enhance the secretion of some insulin-regulated adipocyte cargo, such as LPL.

Next, we treated cells with the Ca<sup>2+</sup> chelator BAPTA-AM, which completely abolished LPL secretion (Fig. 5B). We found that BAPTA treatment caused a reduction in intracellular LPL levels (Fig. 5B). This may be due to enhanced degradation of LPL in the lysosomes, as BAPTA is known to interfere with lysosomal trafficking (Xu and Ren, 2015). Whereas insulin does not significantly increase intracellular Ca<sup>2+</sup> levels (Wang et al., 2014), Ca<sup>2+</sup> is required for insulin signaling in 3T3 cells (Worrall and Olefsky, 2002). Together, these data suggest that LPL and leptin share some upstream signaling regulators, such as the insulin signaling pathway, but rely on separate terminal signaling steps.

### Molecular characterization of LPL storage vesicles

Ca<sup>2+</sup> fulfills many fundamental roles as a secondary messenger in cell physiology (Bootman and Bultynck, 2020), making it difficult to hypothesize a singular role in protein trafficking. However, recent studies have shown that Ca<sup>2+</sup>-dependent protein kinases and phospholipases localized to the Golgi are important for atypical protein secretion (Egea-Jimenez and Zimmermann, 2018). Specifically, PRKDs have been shown to facilitate Golgi vesicle formation and bidirectional trafficking (Bossard et al., 2007). A previous study found that in chemically induced diabetic rats, PRKD cleavage was associated with a reduction in LPL activity (Kim et al., 2009); however, the relationship between different PRKD isoforms, insulin and LPL is unknown. Thus, we measured the effects of several protein kinase inhibitors on insulin-stimulated LPL secretion. The well-characterized pan-protein kinase C

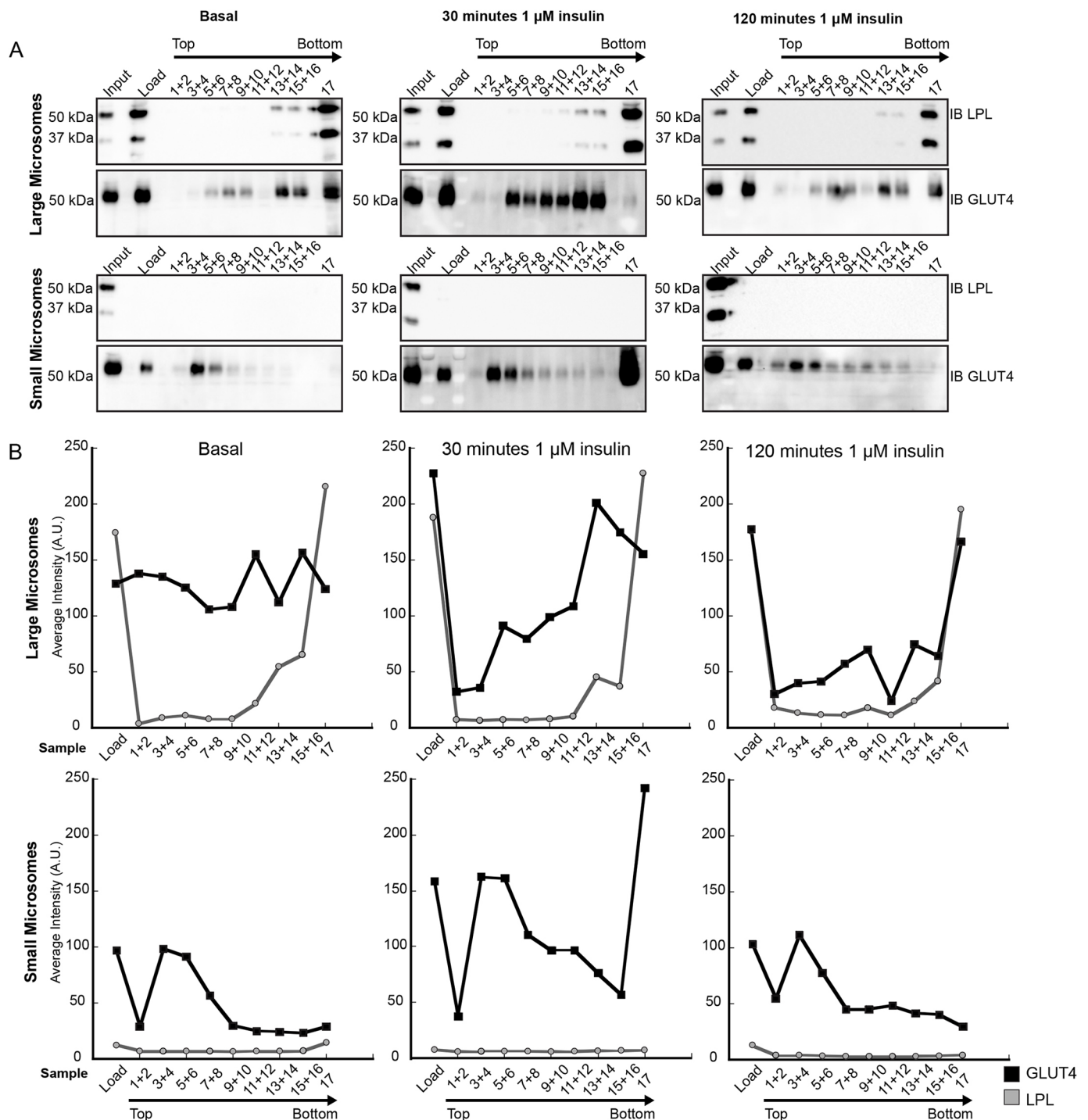


**Fig. 2. LPL and GLUT4 do not fractionate together in 3T3 adipocytes.** (A) Adipocytes were treated with vehicle (basal) or insulin for the indicated times and lysed. Cleared lysate (Input), total large or small microsomal fraction (Load), and pooled fractions are indicated. Whereas GLUT4 shifts between large and small microsomes upon insulin stimulation, LPL does not and remains in the largest of the large microsomes. All experiments were repeated in duplicate. (B) The average band intensity of full-length LPL or GLUT4 from replicate experiments are plotted for each sample ( $n=2$ ).

(PRKC) and PRKD inhibitor Gö6976 reduced LPL secretion by over 25% after 120 min of insulin stimulation but had no effect in unstimulated cells (Fig. 6A). Next, we treated cells with the PRKD-specific inhibitor CRT0066101 (CRT) (Jensen et al., 2016). In insulin-stimulated cells, CRT reduced full-length and cleaved LPL secretion by over 50%, but again had no effect on unstimulated cells (Fig. 6B).

Several PRKD isoforms are found in the Golgi (Pusapati et al., 2009). Both PRKD2 and PRKD3 are major regulators of *trans*-Golgi vesicle transport (Stalder and Gershlick, 2020) and PRKD2 has been linked to insulin signaling in several tissues (Xiao et al., 2018). Thus, we asked whether PRKD2 specifically associated with LPL in adipocytes. We infected mature 3T3-L1 adipocytes with lentiviruses as has been done elsewhere (Carloti et al., 2004)

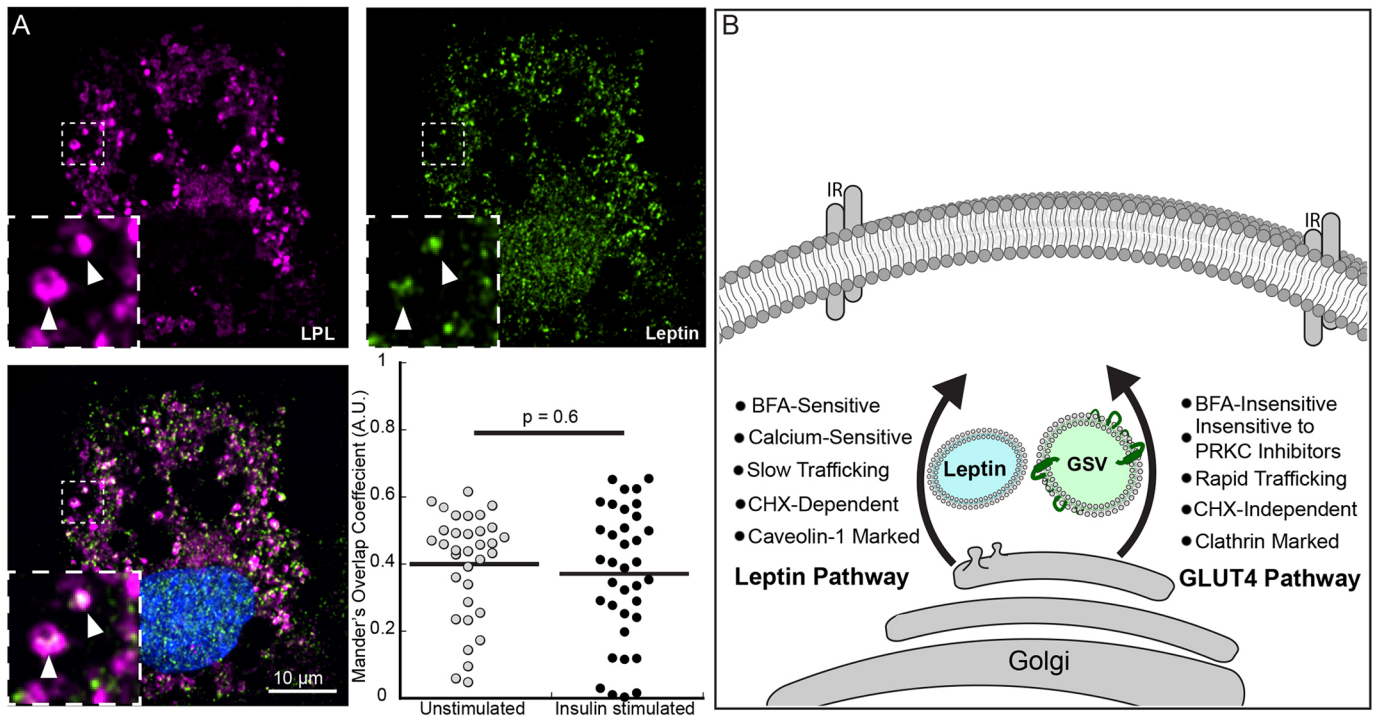


**Fig. 3. Leptin trafficking resembles that of LPL rather than GLUT4 trafficking.** (A) Unstimulated cells were stained for LPL (magenta) and leptin (green). Insets show selected magnified views of the indicated area. Examples of colocalizing puncta are indicated with arrowheads. The Mander's overlap coefficient of LPL overlapping leptin is shown for unstimulated (white) and insulin-stimulated (gray) cells from three biological replicates: basal ( $n=34$ ) insulin-stimulated ( $n=36$ ). A.U., arbitrary units. The  $P$ -value was calculated with a Mann–Whitney  $t$ -test. Scale bar: 10  $\mu\text{m}$ . (B) Comparison of the leptin and GLUT4 pathways. IR, insulin receptor.

carrying either a PRKD2 knockdown (KD) or scramble shRNA and analyzed lysate and medium LPL levels. In scramble cells, LPL secretion was increased by 120 min of insulin treatment, whereas secretion was reduced in PRKD KD cells (Fig. 6C). PRKD2 KD had no effect on LPL secretion in unstimulated cells (Fig. 6C). These results closely resembled the results from our experiments with CRT and confirmed that PRKD2 specifically regulates LPL secretion in adipocytes.

Next, we used sorbitol fractionation to analyze PRKD2 levels in 3T3-L1 adipocytes before and after 120 min of insulin stimulation and found PRKD2 in the same fractions as LPL under basal and insulin-stimulated conditions (see PRKD2 in Fig. 6D and LPL in Fig. 2A). In agreement with this data, we observed that overexpressed PRKD2-V5 colocalized with endogenous LPL in fixed cells (Fig. 6E). In 3D reconstructions, LPL decorated V5-marked Golgi tubules and post-Golgi puncta (Fig. 6E). Following these findings, we investigated the role of PRKD2 partners in insulin-stimulated LPL secretion.

### The role of ARF1 in LPL secretion

Recent studies have identified ARF1 as an essential PRKD partner in Golgi to PM trafficking. Specifically, the isoform PRKD2 is recruited to the Golgi by GTP-bound ARF1 (Pusapati et al., 2009). Whereas ARF1 is generally described as an essential component of the ER to Golgi secretory route, it is also essential in insulin-stimulated post-Golgi vesicle trafficking (Shome et al., 1997; Bottanelli et al., 2017; Kumar et al., 2019). Furthermore, the ARF1 guanine exchange factor (GEF) inhibitor BFA significantly reduces leptin secretion in adipocytes (Wang et al., 2014) and reduces LPL secretion but not intracellular LPL activity (Park et al., 1996). Thus, we asked whether BFA inhibited insulin-stimulated LPL secretion.

We found that BFA completely abolished LPL secretion under insulin-stimulated and basal conditions (Fig. 7A). However, inhibition of ARF1 GEFs by BFA promotes the collapse of the Golgi into the ER, making it a blunt, preliminary tool for dissecting ARF1-dependent trafficking (Bannykh et al., 2005).

Several studies show that BFA does not prevent the secretion of some constitutively secreted cargo that is present in the post-Golgi compartments. For example, in yeast a mature glycosylated form of  $\alpha$ -factor is secreted in BFA-treated cells whereas an immature form is not (Graham et al., 1993). In pancreatic acinar cells, BFA does not prevent the constitutive secretion of pancreatic lipase (De Lisle and Bansal, 1996) or  $\alpha$ -amylase from zymogen granules (Hendricks et al., 1992). LPL secretion requires glycosylation in the ER and *cis*-Golgi. However, essential processing happens in the *medial*- and *trans*-Golgi are not required for LPL secretion (Simsolo et al., 1992). In adipocytes, adiponectin secretion is enhanced by extended insulin treatment (Blümer et al., 2008) and partly blocked by BFA treatment (Wang et al., 2014; Xie et al., 2008). In agreement with those studies, we found that BFA partly reduced the secretion of adiponectin by 75–80% (Fig. S5), in contrast with LPL secretion which was reduced by over 95% following BFA treatment (Fig. 7A).

In addition to BFA, overexpression of a dominant-negative form of ARF1 T31N, which is unable to bind GTP, blocks the trafficking of certain cargo (Jung et al., 2012). GTP hydrolysis is required for PRKD2-dependent tubule formation (Bottanelli et al., 2017) and ARF1 T31N has a reduced capacity for binding PRKD2 (Pusapati et al., 2009). Thus, we asked whether ARF1 was required to facilitate regulated LPL trafficking. To test this, we generated stable 3T3-L1 cell lines expressing ARF1 T31N–GFP or ARF1 wild type (WT)–GFP to test whether heterozygous expression of ARF1 T31N

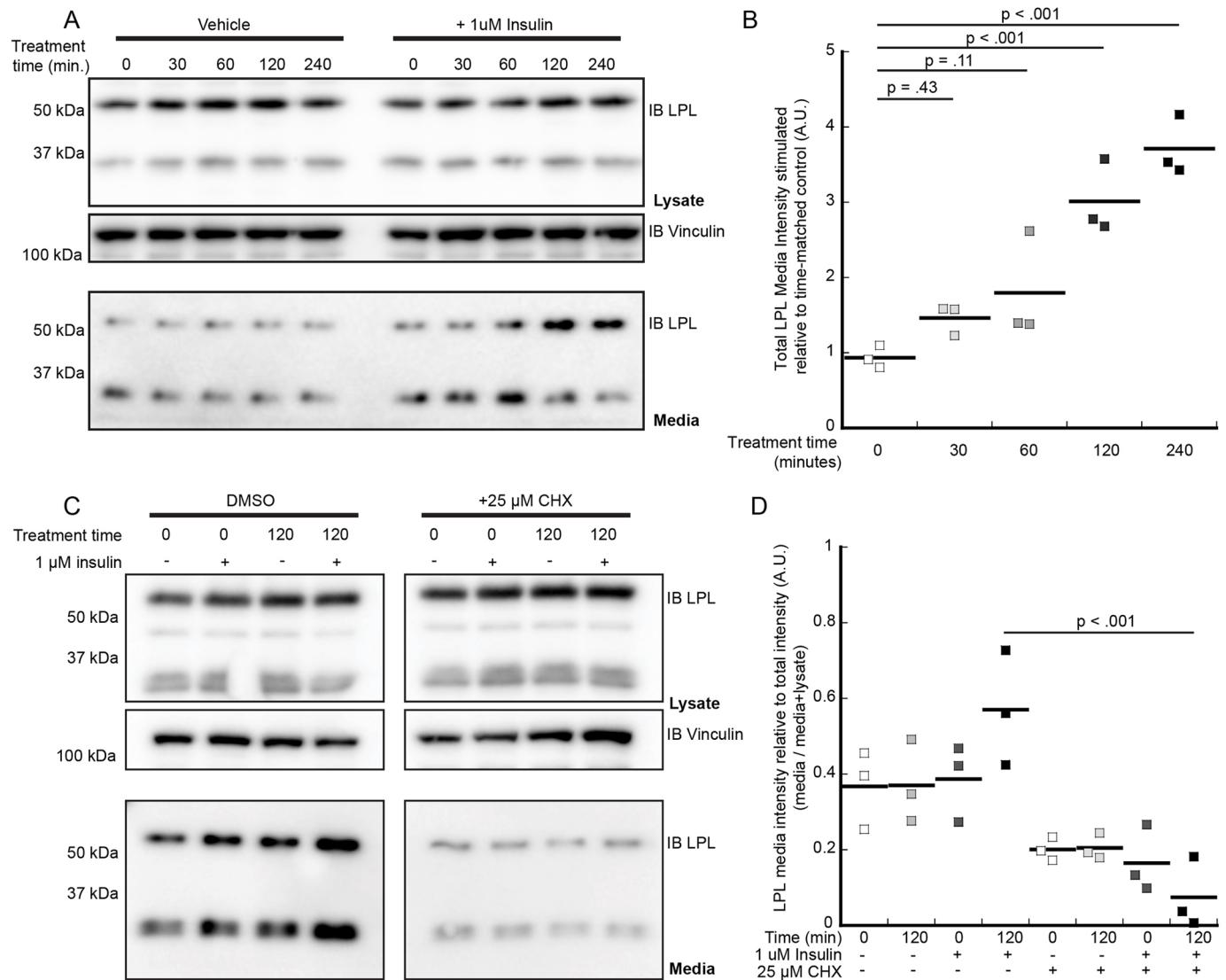


**Fig. 4. Insulin regulates LPL secretion through a translational step.** (A,B) Cells were treated with insulin or vehicle for the indicated times and harvested after 4 h with 15 U/ml heparin. The intensity of total LPL (full-length plus cleaved) was measured and plotted as the band intensity relative to cells treated with vehicle (0 min). *P*-values were calculated by one-way ANOVA with Dunnett's post-hoc test. (C,D) Cells were treated with vehicle or 25  $\mu$ M CHX before treatment with vehicle or insulin, and vehicle or CHX for the indicated times. Full-length LPL bands in media were measured and plotted as media levels relative to total LPL levels (medium or medium plus lysate) under each condition. Significant interactions were calculated with a three-way ANOVA and *P*-values were calculated with Student's *t*-test. All experiments were completed in triplicate. IB, immunoblot.

with endogenous ARF1 WT would affect LPL secretion. In unstimulated cells, there was no difference in LPL secretion between control, ARF1 WT and ARF1 T31N samples (Fig. S6), indicating that unstimulated constitutive secretion may not rely on high ARF1 activity. In contrast, insulin stimulation significantly increased LPL secretion in both control cells and cells overexpressing ARF1 WT relative to the basal state, whereas insulin stimulation had no effect on LPL secretion in cells expressing ARF1 T31N (Fig. 7B). Furthermore, we found that overexpression of ARF1 T31N did not have a significant effect on unstimulated or insulin-stimulated adiponectin secretion (Fig. S7A–D). These results indicate that ARF1 may play a unique role in insulin-stimulated LPL secretion in adipocytes.

We found that ARF1 WT forms distinct ring-like structures overlapping with or adjacent to LPL in unstimulated cells (Fig. 7C). We observed similar structures in cells expressing ARF1 T31N (Figs 7C). Exogenous ARF1 WT and T31N form similar structures in

other cell types (Nakamura et al., 2004). This finding raises the possibility that ARF1 associates with mature LSVs, and ARF1 T31N may affect LSV stability and release rather than LSV formation. The well-defined ARF1 structures we observed led us to examine whether ARF1 localized with PRKD2 in 3T3 adipocytes. To examine the cellular localization of LPL with PRKD2 and ARF1, we transfected cells with ARF1 WT–GFP and PRKD2–V5 and stained for GFP, V5 and endogenous LPL. We found that PRKD2 colocalized with ARF1 in tubular structures abutting LPL marked compartments (Fig. 7D). Our results support the hypothesis that LSVs localize to a specialized insulin-stimulated trafficking site in adipocytes.

## DISCUSSION

LPL is an essential enzyme in the regulation of plasma triglycerides. A loss of LPL activity either due to genetic loss, inhibition or dysfunctional signaling can result in pathological hyperlipidemia, and in individuals with T2D, poor insulin sensitivity correlates with

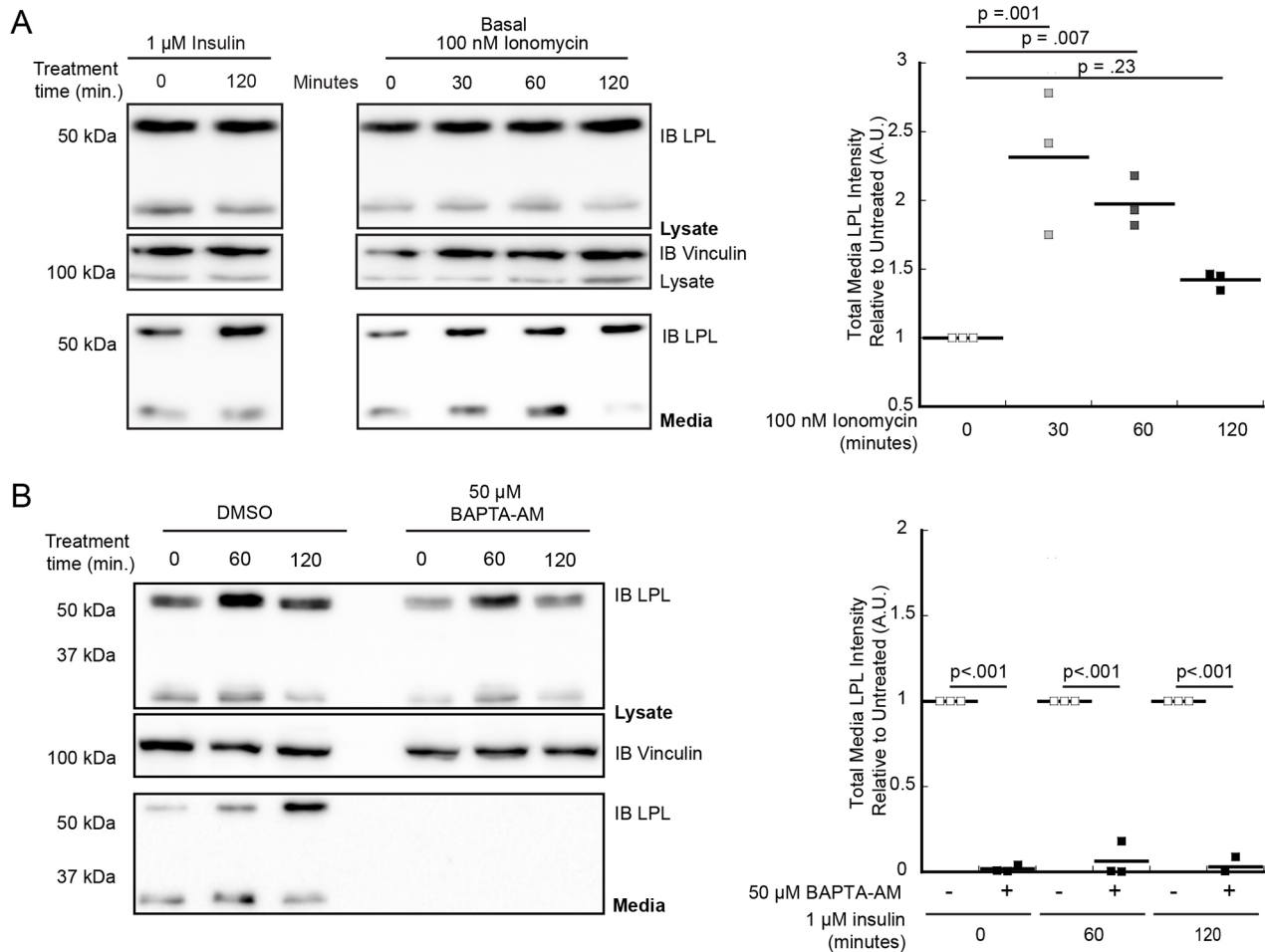


**Fig. 5.  $\text{Ca}^{2+}$  is necessary and sufficient for stimulated LPL secretion.** (A) Cells were treated with either insulin (left) or ionomycin (right) for the indicated times. Untreated cells (0) were treated with vehicle alone. Total medium LPL (full-length and cleavage) was measured and plotted relative to values in untreated cells (0). *P*-values were calculated by one-way ANOVA with Dunnett's post-hoc test. (B) Cells were pre-treated with DMSO or BAPTA-AM for 30 min before the addition of either vehicle or insulin for the indicated times. Total media LPL is plotted. Significant interactions were calculated with a two-way ANOVA and *P*-values were calculated with Šidák-corrected pairwise tests. All experiments were repeated in triplicate. IB, immunoblot.

low plasma LPL activity (Huang et al., 2013). However, a mechanism for insulin-dependent LPL activity has remained elusive. In the 1980s a series of studies described the biosynthesis (Vannier et al., 1989) and regulated release of LPL in 3T3-L1 adipocytes (Semenkovich et al., 1989), showing that insulin regulates LPL activity at post-translational steps. A decade later, another study showed that insulin regulates LPL trafficking through both the AKT and mTORC pathways (Kraemer et al., 1998). Although GLUT4 exhibits well-described insulin-stimulated trafficking, subcellular fractionation has shown that LPL trafficking is unlike GLUT4 trafficking in rat adipocytes (Roh et al., 2001). Instead, Kim et al. (2009) identified PRKD as a unique regulator of cardiac LPL secretion in diabetic rats. Together, these findings conclusively implicated insulin in a regulated LPL trafficking pathway.

Several recent publications have advanced our understanding of LPL trafficking. In a series of publications, the Burd group identified a novel mechanism of soluble protein sorting specific to SM carriers originating in the *trans*-Golgi. One of these cargos, SDC1, had been previously implicated in LPL release from adipocytes (Deng et al., 2018, 2016; Reizes et al., 2006). In a subsequent study, Sundberg et al. (2019) showed that LPL trafficking required SDC1 and SM carriers for TGN to PM trafficking. Our group recently described a novel oligomerization of

LPL in a helical structure. We found that LPL formed tube-like filaments that colocalized with SDC1 in adipocytes, and that disruption of a critical helical interface disrupted the tube-like appearance of the LPL in cells (Gunn et al., 2020). Together, these publications indicate that LPL secretion follows a unique regulated pathway in cells such as adipocytes.

We observed that LPL localizes to a unique secretory compartment in distal structures throughout the cell, unlike what is seen for GLUT4, which is concentrated in the perinuclear region under basal conditions or at the PM during insulin stimulation (Fig. 1). We found that LPL colocalizes with Cav1, the Golgi marker GGA2 and the endosome marker RAB10 (Figs 1). To our surprise, only the colocalization of LPL with clathrin changed after insulin stimulation. This decreased colocalization may be caused by a shift from LPL bulk flow to regulated trafficking with SDC1. These results led us to examine LPL using subcellular fractionation. We found that LPL fractionated in large structures that did not respond to insulin stimulation as GLUT4 did (Fig. 2). Following insulin stimulation, GSVs are trafficked from large perinuclear structures to small endosomal structures (Kupriyanova et al., 2002). In contrast, LPL did not undergo exchange between fractions containing differently sized structures. Between these results, it is tempting to interpret these data as an indication that LPL is



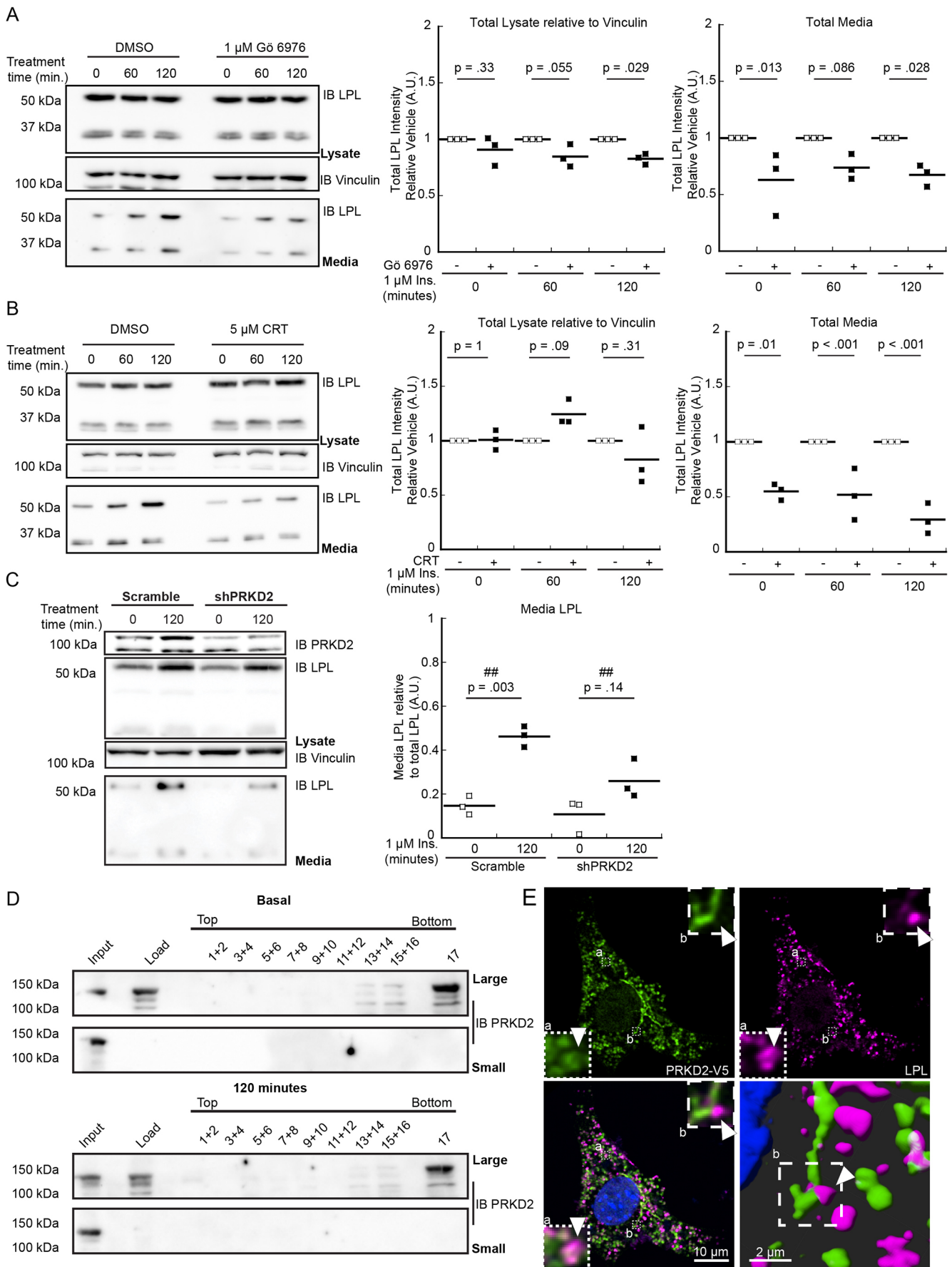


Fig. 6. See next page for legend.

**Fig. 6. Golgi-localized protein kinase D is required for insulin stimulated LPL trafficking.** (A) Cells were pre-treated with DMSO or GO6976 for 30 min before treatment with vehicle or insulin for the indicated times. Total LPL (full-length plus cleaved) is plotted relative to values in vehicle-treated control. (B) Cells were pre-treated with CRT0066101 for 30 min before the addition of either vehicle or insulin for the indicated times. Total LPL is plotted as in A. Secretion assays were repeated in triplicate. (C) Lentiviral expression of an shRNA targeting PRKD2 in 3T3-L1 cells reduces insulin-stimulated LPL secretion versus cells expressing scramble shRNA. Full-length LPL in media samples relative to total full-length LPL (medium plus lysate) is plotted for three replicates experiments. The interaction between the scramble and shPRKD2 group is shown ( $^{##}P=0.008$ ). (D) Fractionated cells were treated as in Fig. 2 and western blots were probed for PRKD2. Fractionations were repeated twice. (E) A representative image of a 3T3-L1 adipocyte immunostained for PRKD2-V5 (green) and endogenous LPL (magenta). A 3D Imaris rendering is shown. Insets show selected magnified views of the indicated area. Arrowheads highlight an example of LPL decorating the PRKD2-marked tubule. Significant interactions were calculated with a two-way ANOVA and *P*-values were calculated with Šidák-corrected pairwise tests. IB, immunoblot.

trafficked in stable LSVs without undergoing the extensive sorting that GLUT4 does. However, live-cell imaging experiments are necessary to clarify the temporal association of LPL and with these markers and compartments.

After observing that GLUT4 trafficking did not resemble LPL trafficking, we turned to leptin as an alternative model of insulin-stimulated trafficking. Using microscopy, we found that LPL vesicles more closely resembled leptin vesicles than GLUT4 vesicles and we hypothesized that certain leptin-trafficking effectors might also affect LPL secretion (Fig. 3). We found that insulin-stimulated LPL secretion requires a biosynthetic step, but that insulin does not regulate LPL biosynthesis itself (Fig. 4). We found that insulin enhanced LPL secretion over the course of several hours, significantly more slowly than the rate of change for insulin-stimulated GLUT4 trafficking (Brewer et al., 2014). Plasma TG and plasma glucose levels rise following a meal. In healthy individuals, postprandial plasma glucose levels drop more quickly than postprandial plasma TG levels (Lambert and Parks, 2012; Morrison et al., 2018). Thus, in a physiological context adipocyte LPL secretion may lag behind GLUT4 trafficking to prioritize glucose uptake for immediate use over TG uptake for storage. Interestingly, insulin stimulation can be bypassed through  $Ca^{2+}$  influx suggesting that insulin is important for a trafficking step independent of LSV maturation (Fig. 5). Given the role of PRKD in this process, insulin may mediate one or more events including a  $Ca^{2+}$ -regulating signaling step.

Insulin does not significantly raise intracellular  $Ca^{2+}$  levels in 3T3 cells (Wang et al., 2014). However,  $Ca^{2+}$  is essential for signaling events immediately downstream of insulin receptor signaling (Worrall and Olefsky, 2002).  $Ca^{2+}$  loading in myoblasts increases PM GLUT4 levels and  $Ca^{2+}$  chelation with BAPTA-AM blocks GLUT4 trafficking (Li et al., 2014). In contrast, whereas insulin-stimulated leptin secretion is blocked by BAPTA,  $Ca^{2+}$  loading by ionomycin is not sufficient to stimulate leptin secretion (Wang et al., 2014). Both phospholipases C (PLC) and D (PLD) respond to  $Ca^{2+}$  flux by producing diacylglycerol (DAG) and phosphatidic acid (PA) (Jenkins and Frohman, 2005; Kanaho et al., 1992). These signaling lipids recruit protein kinases to the membrane. Specifically, PRKC isoforms continue to activate PLC and PLD, as well as PRKD (Jenkins and Frohman, 2005); and, simultaneously, insulin activates PRKC directly through PDK1 (Boucher et al., 2014). These parallel and cyclic signaling events generate DAG and PA to recruit machinery such as PRKD to the Golgi membrane. In myocytes, PRKD is required for LPL

trafficking (Kim et al., 2009) and, in HeLa cells, PRKD2 is involved in MMP trafficking (Eiseler et al., 2016). We found that inhibition or knockdown of PRKD2 reduced insulin-stimulated but not unstimulated LPL secretion (Fig. 6). Thus, PRKD2 is critical for regulated LPL secretion in adipocytes.

We also found that BFA entirely blocked LPL secretion (Fig. 7) in contrast with what was seen for adiponectin, which is only partly blocked by BFA (Fig. S5). BFA inactivates the small GTPase ARF1 by inhibiting ARF1 GEFs (D'Souza-Schorey and Chavrier, 2006). ARF1 classically plays a central role in regulating ER to Golgi trafficking (Dascher and Balch, 1994) but has also emerged as a unique regulator of some Golgi to PM transport (Bottanelli et al., 2017). For example, whereas BFA treatment abolishes polarized SDC1 trafficking (Miettinen et al., 1994), BFA treatment does not inhibit the insulin-stimulated trafficking of mature GSVs (Martin et al., 2000) and only partly inhibits adiponectin trafficking (Xie et al., 2008). Because SDC1 is found in LSVs (Gunn et al., 2020; Sundberg et al., 2019) and we show that LSV trafficking is ARF1-dependent, it stands to reason that SDC1 sorting is ARF1-dependent in 3T3-L1 adipocytes.

In our hands, BFA entirely blocked LPL secretion (Fig. 7), indicating that ARF1 GEFs are required for LPL trafficking. However, expression of a dominant-negative ARF1 lacking GTPase activity reduced insulin-stimulated LPL secretion without affecting unstimulated LPL secretion (Fig. 7; Fig. S6). Thus, sufficient ARF1 GTPase activity is essential for regulated LPL trafficking but not for the low levels of basal secretion observed in unstimulated cells. Future studies should use live-cell imaging to further describe the roles of ARF1 WT and dominant-negative ARF1 on subcellular LPL trafficking.

Our microscopy studies (Fig. 7) show that PRKD2, LPL and ARF1 localize to many of the same structures in adipocytes. Our findings show that  $Ca^{2+}$ , insulin, and both ARF1 and PRKD2 are required for LPL secretion from these structures. In other cell types, PRKD2 and ARF1 associate and regulate membrane budding at the TGN (Eiseler et al., 2016; Hausser et al., 2005). In addition, ARF1 regulates endosome trafficking in cargo sorting (Nakai et al., 2013). Thus, it is possible that ARF1 participates in LPL sorting in the endosomal network. Further studies are necessary to identify specific roles and to demonstrate a direct relationship between ARF1 and PRKD2 in insulin-stimulated LPL trafficking.

In conclusion, to the best of our knowledge our study provides the first evidence of an insulin-regulated Golgi to PM trafficking pathway in adipocytes. A number of excellent proteomics (Humphrey et al., 2013; Wang et al., 2004) and transcriptomics (Wang et al., 2006) studies have identified insulin-regulated pathways that could serve the basis for future investigations of regulated trafficking. These studies should identify cargo unique to insulin-regulated Golgi to PM secretory vesicles and examine the involvement of membrane lipids in this process (Fig. 8).

## MATERIALS AND METHODS

### Cell culture

3T3-L1 adipocytes (American Type Culture Collection; Manassas, VA, USA; CL-173) were maintained in Dulbecco's modified Eagle's medium (DMEM; Gibco; 11965) containing 10% fetal bovine serum (FBS) (Avantor Seradigm; Radnor, PA, USA),  $1\times$  L-glutamine (Gibco; 35050) and  $1\times$  penicillin/streptomycin (Gibco; 15070). 3T3 cells were differentiated as previously described (Gunn et al., 2020). Briefly, cells were maintained in DMEM containing 10% premium FBS (Avantor Seradigm; Premium Grade FBS),  $1.5\ \mu\text{g/ml}$  insulin (Gibco; 12585),  $0.5\ \text{mM}$  IBMX (Sigma-Aldrich; I5879),  $1\ \mu\text{M}$  dexamethasone (Sigma-Aldrich; D4902) and  $2\ \mu\text{M}$

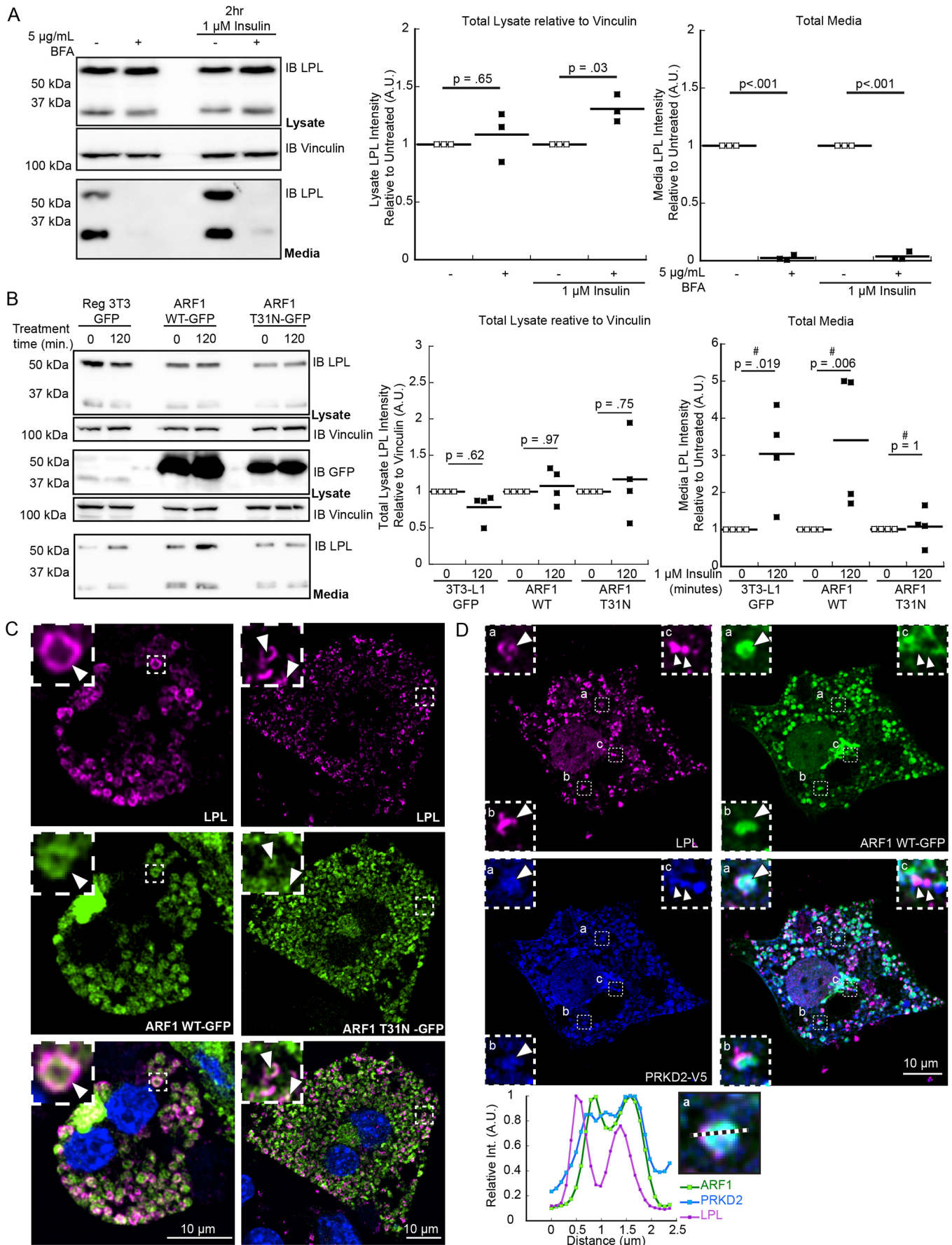


Fig. 7. See next page for legend.

**Fig. 7. ARF1 is essential for LPL secretion.** (A) Cells were treated with 5  $\mu\text{g/ml}$  BFA for 30 min before insulin was added for 0 or 2 h. Graphs show full-length medium and lysate LPL levels relative to untreated controls for three replicate experiments. Lysate LPL levels: +/- BFA=109% $\pm$ 21; insulin-stimulated +/- BFA=131% $\pm$ 12. Medium LPL levels: +/- BFA=3% $\pm$ 2; insulin-stimulated +/- BFA=4% $\pm$ 4. Significant interactions were calculated with a two-way ANOVA and *P*-values were calculated with Šidák-corrected pairwise tests. (B) 3T3-L1 adipocytes expressing either GFP, or GFP-tagged ARF1 WT or ARF1 T31N were treated with vehicle or 1  $\mu\text{M}$  insulin for the indicated times, and media and lysates were collected. Overexpression of an inactive GDP-bound ARF1 mutant (T31N) reduces LPL secretion in insulin-stimulated adipocytes. The ARF1 mutant T31N is poorly expressed, and ARF1 WT is overexpressed (IB GFP). Full-length LPL band intensity relative to unstimulated cells are shown for four replicate experiments. The interaction between the 3T3-L1, ARF1 WT and T31N ARF1 groups is shown ( $\#P=0.05$ ). (C) WT and T31N ARF1 (green) localize to LPL (magenta) vesicles in 3T3 adipocytes. Insets show selected magnified views of the indicated area. Arrowheads highlight ring-like structures containing ARF1 and LPL. (D) In adipocytes, LPL (magenta), ARF1 WT (green), and PRKD2 (blue) localize to tubular structures throughout the cell. Insets show selected magnified views of the indicated area. Arrowheads highlight LPL decorating PRKD2-marked structures. To depict the colocalization of PRKD2, LPL and ARF1, the intensity of a bisecting line (dotted line) from a single Z-plane in box a was plotted for PRKD2, LPL and ARF1. All intensities were normalized to 1. Scale bars: 10  $\mu\text{m}$ . Significant interactions were calculated with a two-way ANOVA and *P*-values were calculated with Šidák-corrected pairwise tests. IB, immunoblot.

rosiglitazone (Sigma-Aldrich; R2408) (M2 medium) for 48 h, in DMEM containing 10% premium FBS and 1.5  $\mu\text{g/ml}$  insulin (M3 medium) for 48 h, and again in M2 medium for 48 h before maintenance in M3 medium until use. Cells were grown until at least day 10 of differentiation before use in experiments. At 16 h before use, cells were rinsed in PBS and grown overnight in DMEM containing 0.2% bovine serum albumin (BSA) (Sigma-

Aldrich; A8806), 1 $\times$  L-glutamine and 1 $\times$  penicillin/streptomycin. Cells were rinsed with phosphate-buffered saline (PBS) and grown in DMEM containing 0.02% BSA for all LPL secretion western blot and mRNA isolation experiments; cells were grown in DMEM containing 0.2% BSA during all other experiments.

### Fluorescence microscopy

Cells were grown and treated as described previously (Gunn et al., 2020). Briefly, cells were plated on #1.5 coverslides (Fisher; 12-545-81P) coated with poly-D-lysine (Sigma-Aldrich; P7405) and rat tail collagen (Gibco; A1048301). Following treatments, cells were washed with PBS and fixed with 4% paraformaldehyde for 5–10 min at 22°C. Cells were washed with PBS three times for 10 min each and permeabilized with 0.2% Triton X-100 (Fisher; T9284) in blocking solution (PBS, 5% BSA, 100 mM glycine) for 15 min. Next, cells were blocked for 30 min at 22°C with 5% donkey serum (Sigma-Aldrich; D9663) in blocking solution. Cells were stained in parallel with anti-LPL (1:40; R&D systems; AF7197) overnight at 4°C followed by PBS washes and staining with anti-goat-IgG conjugated to Alexa Fluoro 594 (AF594) (1:1000; Invitrogen; A-21468) for 1 h at 22°C. Next, cells were washed with PBS and stained overnight with anti-GLUT4 (1:1000; Abcam; ab654), anti-caveolin 1 (1:400; Cell Signaling Technologies (CST); 3238S), anti-clathrin (1:50; CST; 4796S), anti-syntaxin 6 (1:50; CST; 2869T), anti-V5 (1:1500; Biorad; MCA1360), anti-GGA2 (1:100; SCBT; sc-133147), anti-golgin-97 (1:200; CST; 13192S), anti-EEA1 (1:200; CST; 3288S) or anti-GFP (1:1000; Invitrogen; A11122) antibodies. Finally, cells were washed with PBS and stained with donkey-anti-rabbit-IgG conjugated to Alexa Fluoro 488 (AF488) (1:1000; Invitrogen; A-21206) for 1 h at 22°C. Cells stained for V5 tag were also stained with anti-mouse-IgG conjugated to Alexa Fluoro 405 (1:1000; Invitrogen; 31553). Samples stained with AF488 and AF594 were also stained with DAPI (10  $\mu\text{M}$ ; Invitrogen; D9542) in PBS and mounted in Prolong Diamond antifade (Invitrogen; P36961).

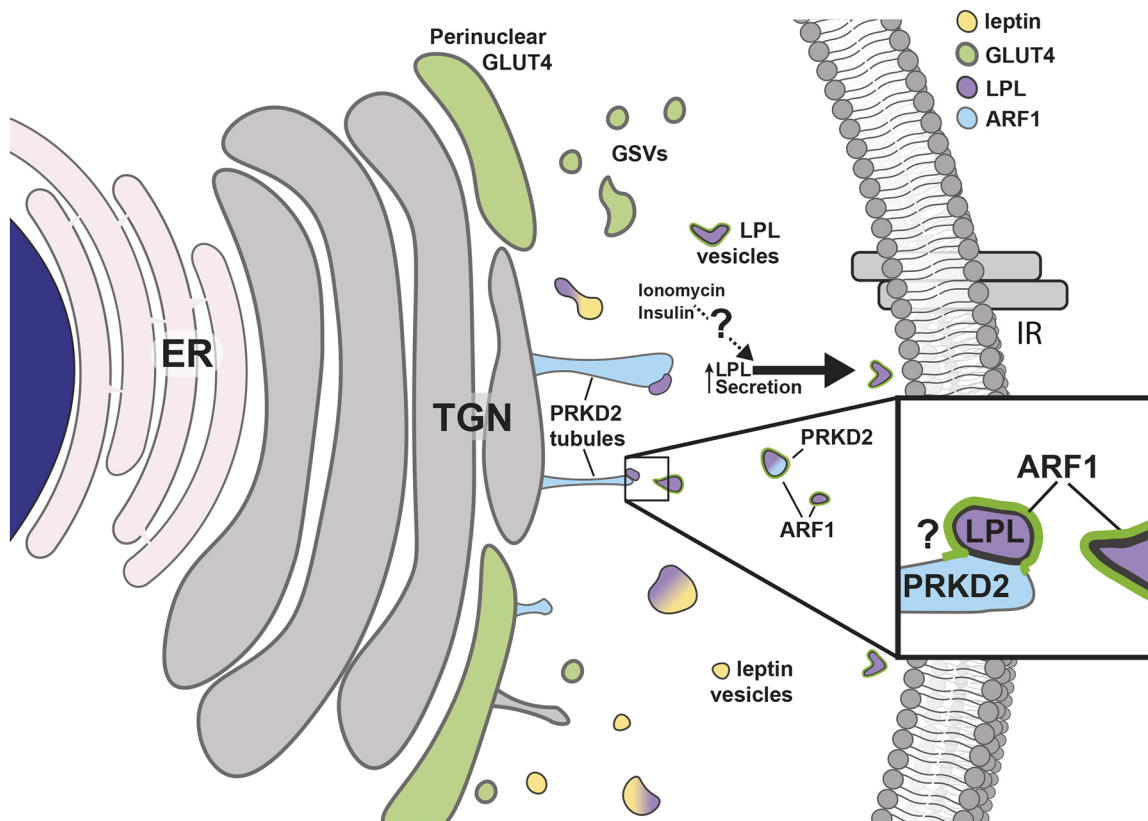


**Fig. 8. A hypothetical model of LPL secretion.** In adipocytes, LPL is trafficked to distinct post-Golgi microdomains marked by Cav1. Some LSVs overlap with leptin vesicles and GSVs. These microdomains are found at projections marked by PRKD2 and ARF1. LPL is stored until insulin signaling (via insulin receptors; IR) or ionomycin stimulation induce LPL exocytosis. LSVs localize to TGN and endosome markers. It is unclear how ARF1 and PRKD2 directly contribute to LSV trafficking and LPL secretion.

Fixed cells were imaged on a Zeiss LSM 710 spectral laser scanning confocal microscope equipped with a Plan Apo 40×/1.4 NA oil objective. Acquisition settings initially were selected to avoid more than ~1% pixel saturation in a given field. Only cells displaying LPL puncta were selected for imaging. All images were acquired with the same LPL channel acquisition settings. Each group of images were acquired with different settings for the second channel (green) to accommodate variability in expression and staining of the second target. Within each group, all acquisition settings were kept the same. Acquired Z-stacks were deconvolved in AutoQuant X3 (Media Cybernetics, Rockville, MD). For analysis, single cells were cropped and channels were median filtered and then thresholded for the brightest pixels for a given group (i.e. top 5% of pixels in each channel). Colocalization was analyzed on thresholded images in Fiji (Schindelin et al., 2012) using the JaCoP plugin to measure the Mander's overlap coefficient. This method generated overlap coefficient values between  $0.058 \pm 0.05$  ( $\pm$ s.d.; negative control generated by flipping images horizontally and vertically) and  $0.87 \pm 0.05$  (positive control generated by measuring the overlap of GFP with anti-GFP antibody). Three-dimensional analysis was undertaken in Imaris (<https://imaris.oxinst.com>).

### Lentivirus production, infection and transfection, and molecular cloning

For viral production, HEK293T (American Type Culture Collection; CRL-3216) cells were maintained in DMEM containing 10% FBS,  $1 \times$  L-glutamine and  $1 \times$  penicillin/streptomycin. Cells were grown to confluence and transfected with  $9 \mu\text{g}$  of viral expression vector [pLV-EF1A-Blast or pLKO.1-CMV carrying scramble (Sigma-Aldrich; SHC002) or PRKD2 shRNA (Sigma-Aldrich; SHCLNG-NM\_178900 TRCN0000322347)],  $6 \mu\text{g}$  of psPAX2-CMV and  $3 \mu\text{g}$  of pCMV-VSV-G. psPAX2-CMV and pCMV-VSV-G were kind gifts of the Mohlke lab (University of North Carolina at Chapel Hill, Chapel Hill, NC, USA). pLV-EF1A-Blast was a kind gift of the Davis Lab (University of North Carolina at Chapel Hill, Chapel Hill, NC, USA). After 24 h medium was exchanged for DMEM containing 20% FBS,  $1 \times$  L-glutamine, and  $1 \times$  penicillin/streptomycin and media was collected at 48 and 72 h post transfection. Viral medium was added to 3T3-L1 pre-adipocytes with  $10 \mu\text{g}/\text{ml}$  polybrene (Santa Cruz Biotechnology; sc-134220) added. After 24 h, the medium was changed, and cells were selected with either  $2 \mu\text{g}/\text{ml}$  puromycin (Thermo Fisher Scientific; NC9138068) or  $10 \mu\text{g}/\text{ml}$  blasticidin (Invitrogen; NC9016621).

The plasmids RAB4-GFP, RAB10-GFP and LAMP1-GFP were gifts from Prasanna Satpute-Krishnan (USUHS, Bethesda, MD, USA). Full-length GFP-tagged ARF1 was cloned from mouse cDNA. pLX304-PRKD2-V5 and pLX304-ARF6-V5 were purchased from the University of North Carolina at Chapel Hill Lenti-cDNA Core facility (ARF6 ORFeome clone #101925986, GenBank accession BC008918; PRKD2 ORFeome clone #101931358, GenBank accession NM\_001079881). All GFP-tagged constructs were amplified and cloned into a pLV-EF1A-Blast vector using Gibson Assembly (New England Biolabs; Ipswich, MA, USA). The resultant plasmids were used for transfection or lentiviral production.

For transient transfection, day 10 3T3-L1 adipocytes were electroporated using a Lonza Nucleofector 2 device under program A-033 with a total of  $10 \mu\text{g}$  of DNA resuspended in Mirus Ingenio transfection solution (Mirus Bio; Madison, WI, USA) as per the manufacturer's instructions.

### Western blotting

For whole-cell lysates, cells were lysed using modified radio immunoprecipitation buffer (50 mM Tris-HCl pH 7.5, 150 mM NaCl, 1% Triton X-100, 1% SDS) with grinding. Lysates were rocked at  $22^\circ\text{C}$  for 30 min and spun down ( $6000 \text{ g}$  for 2 min) to pellet insoluble material. Lysate concentrations were then measured with a bicinchoninic acid assay (BCA). Equal amounts of all lysates were combined with  $5 \times$  SDS plus dithiothreitol (DTT) loading dye, heated at  $72^\circ\text{C}$ , and resolved by SDS-PAGE. For blots of media, media was removed and spun down at  $4000 \text{ g}$  for 10 min at  $4^\circ\text{C}$  and supernatant was moved to a fresh tube. Equal volumes of media were combined with  $5 \times$  SDS plus DTT loading dye, heated at  $72^\circ\text{C}$ , and resolved by SDS-PAGE. For western blotting, SDS-PAGE gels were transferred to PVDF membranes and blocked for 1 h in 5% milk in Tris-buffered saline

with 0.1% Tween 20 (TBST). Membranes were then probed overnight at  $4^\circ\text{C}$  with anti-LPL (1:200; R&D Systems; AF7197), anti-GFP (1:1000; CST; 2955), anti-GLUT4 (1:2500; Abcam; ab654), anti-PRKD2 (1:1000; ProteinTech; 11623-1-AP) or anti-adiponectin (1:500; Invitrogen; PA1-054) antibodies. Next, blots were washed in TBST and probed with the appropriate horseradish peroxidase (HRP)-conjugated anti-goat-IgG (1:1000; R&D systems; AF7197), HRP-conjugated anti-mouse-IgG (1:5000; Southern Biotech; OB1030-05 or OB6440-05). Blots were finally washed with TBST and revealed with enhanced chemiluminescence substrate solution (Advansta; K-12045-D50).

To quantify western blots, the highest exposure before pixel saturation was selected and the intensity of each background-subtracted band was measured in Fiji software. Lysates samples intensities were measured relative to their respective loading control. LPL band intensity was measured as either full-length LPL alone or full-length LPL plus the LPL cleavage product, as specified in figure legends.

### Cell fractionation

Cells were fractionated as described elsewhere with modifications (Rossi et al., 2018; Sadler et al., 2016). Briefly, cells were differentiated and grown in DMEM containing 0.2% BSA overnight before harvesting. On the day of harvesting, cells were treated with  $1 \mu\text{M}$  insulin for the indicated times and then washed with ice-cold PBS containing 2.5 mM EDTA and protease inhibitor cocktail (Pierce; PI88266) and all subsequent steps were conducted at  $4^\circ\text{C}$ . Cell pellets were lysed in resuspension buffer (14% sorbitol, 20 mM HEPES pH 7.2,  $1 \times$  Pierce protease inhibitor cocktail) through 25G and 26G needles. Next, cell lysates were centrifuged at  $500 \text{ g}$  for 10 min to pellet nuclei and other large debris. Supernatants were removed and centrifuged at  $30,000 \text{ g}$  for 15 min to separate large and small structures. The resuspended pellet (large) and supernatant (small) from this step were further purified by layering over a 20% sorbitol cushion and centrifuging at  $100,000 \text{ g}$  for 90 min in a TLA100.3 rotor. Pellets from this step were suspended in resuspension buffer and layered on top of a 20–40% sorbitol gradient. Samples were then centrifuged at  $71,000 \text{ g}$  for 2 h in an SW40-Ti rotor, and de-fractionated from top to bottom (small to large). De-fractionated samples were mixed (i.e. samples 1 and 2, samples 3 and 4) and diluted in  $1 \times$  PBS before pelleting at  $16,000 \text{ g}$  for 90 min. Pellets were resuspended in  $5 \times$  SDS plus DTT and prepared for analysis by western blotting.

### RT-qPCR

For RT-qPCR, RNA samples were extracted as with Trizol reagent (Invitrogen; 15596026). RNA was quantified and  $500 \text{ ng}$  RNA was reverse transcribed to generate cDNA using the iScript cDNA synthesis kit (Biorad; 1708890). For qPCR,  $25 \text{ ng}$  of the resulting cDNA was combined with the following primer pairs and SYBER Select master Mix (Applied Biosystems; 4472908). The following exon-spanning primers were used for qPCR: Gapdh (F, 5'-GTATGACTCCACTCACGGCAA-3'; R, 5'-GGTCTCG-CTCCTGGAAGATG-3'), LPL (F, 5'-GCCAGCAACATTATCCAGT-3'; R, 5'-GGTCAGACTTCTGCTACGC-3'). RT-qPCR was performed using an applied biosystems QuantStudio Flex 6 system (Applied Biosystems). All samples were analyzed in technical and biological triplicates.

### Small-molecule studies

For intracellular  $\text{Ca}^{2+}$  studies, the  $\text{Ca}^{2+}$  chelator BAPTA-AM (ApexBio; B4758; Houston, TX, USA) and the ionophore ionomycin (Sigma-Aldrich; I9657-1MG) were prepared in DMSO and stored at  $-20^\circ\text{C}$  until use. For kinase inhibitor studies, the protein kinase C pan inhibitor G66976 (ApexBio; A8341) and protein kinase D inhibitor CRT0066101 (Sigma-Aldrich; SML1507) were suspended in DMSO and stored at  $-20^\circ\text{C}$  until use. For ARF1 studies, the inhibitor BFA (Sigma-Aldrich; B7651) was stored in methanol and diluted in DMSO for use. For translation studies, the translation inhibitor CHX (Sigma-Aldrich; C7698) was suspended in DMSO and stored at  $-20^\circ\text{C}$  until use.

### Statistics

All quantified data included three or four biological replicate experiments. Data were analyzed in Prism 9 (GraphPad) and graphed in KaleidaGraph. Statistical significance ( $P < 0.05$ ) was calculated using an unpaired two-tailed

*t*-test or Mann–Whitney test for two-sample analyses, or analysis of variance (ANOVA) for multiple analyses. The Dunnett post-hoc test was used for one-way ANOVA and the Šidák-corrected pairwise test was used for two-way ANOVA pairwise comparisons. When variance is shown or discussed it is reported as the standard deviation.

#### Acknowledgements

We are deeply thankful to Dr Patrick Brenwald and Dr Guendalina Rossi (University of North Carolina at Chapel Hill, Chapel Hill, NC) for their help in completing fractionation experiments and in preparation of this manuscript. We also thank Dr Stephanie Gupton (University of North Carolina at Chapel Hill, Chapel Hill, NC) for guidance on microscopy and in the preparation of this manuscript. We thank Dr Rick Baker (University of North Carolina at Chapel Hill, Chapel Hill, NC) for help in preparing this manuscript. Finally, we acknowledge the editorial assistance of the NC Translational and Clinical Sciences (NC TraCS) Institute, which is supported by the National Center for Advancing Translational Sciences (NCATS), National Institutes of Health, through Grant Award Number UL1TR002489.

#### Competing interests

The authors declare no competing or financial interests.

#### Author contributions

Conceptualization: B.S.R.; Methodology: B.S.R., S.B.N.; Software: C.Q.Y.; Formal analysis: B.S.R., C.Q.Y.; Investigation: B.S.R., C.Q.Y.; Resources: S.B.N.; Data curation: B.S.R., C.Q.Y.; Writing - original draft: B.S.R.; Writing - review & editing: B.S.R., S.B.N.; Visualization: B.S.R.; Supervision: S.B.N.; Project administration: B.S.R., S.B.N.; Funding acquisition: S.B.N.

#### Funding

This work was supported by the National Institutes of Health [5 F31 DK122728-02 to B.S.R.; 2 R01 HL125654 06 to S.B.N.] and the University of North Carolina at Chapel Hill (UNC) SOM Office of Research Emerging Challenges in Biomedical Research Pilot Award. Deposited in PMC for release after 12 months.

#### Peer review history

The peer review history is available online at <https://journals.biologists.com/jcs/article-lookup/doi/10.1242/jcs.258734>

#### References

- An, D., Pulini, T., Qi, D., Ghosh, S., Abrahami, A. and Rodrigues, B. (2005). The metabolic "switch" AMPK regulates cardiac heparin-releasable lipoprotein lipase. *Am. J. Physiol. Endocrinol. Metab.* **288**, E246–E253. doi:10.1152/ajpendo.00211.2004
- Bannykh, S. I., Plutner, H., Matteson, J. and Balch, W. E. (2005). The role of ARF1 and Rab GTPases in Polarization of the Golgi Stack. *Traffic* **6**, 803–819. doi:10.1111/j.1600-0854.2005.00319.x
- Blümer, R. M. E., van Roomen, C. P., Meijer, A. J., Houben-Weerts, J. H. P. M., Sauerwein, H. P. and Dubbelhuis, P. F. (2008). Regulation of adiponectin secretion by insulin and amino acids in 3T3-L1 adipocytes. *Metabolism* **57**, 1655–1662. doi:10.1016/j.metabol.2008.07.020
- Bootman, M. D. and Bultynck, G. (2020). Fundamentals of cellular calcium signaling: a primer. *Cold Spring Harbor Perspect. Biol.* **12**, a038802. doi:10.1101/cshperspect.a038802
- Bossard, C., Bresson, D., Polishchuk, R. S. and Malhotra, V. (2007). Dimeric PKD regulates membrane fission to form transport carriers at the TGN. *J. Cell Biol.* **179**, 1123–1131. doi:10.1083/jcb.200703166
- Bottanelli, F., Kilian, N., Ernst, A. M., Rivera-Molina, F., Schroeder, L. K., Kromann, E. B., Lessard, M. D., Erdmann, R. S., Schepartz, A., Baddeley, D., et al. (2017). A novel physiological role for ARF1 in the formation of bidirectional tubules from the Golgi. *Mol. Biol. Cell* **28**, 1676–1687. doi:10.1091/mbc.e16-12-0863
- Boucher, J., Kleinriders, A. and Kahn, C. R. (2014). Insulin receptor signaling in normal and insulin-resistant states. *Cold Spring Harb. Perspect. Biol.* **6**, a009191. doi:10.1101/cshperspect.a009191
- Brewer, P. D., Habtmichael, E. N., Romenskaia, I., Mastick, C. C. and Coster, A. C. F. (2014). Insulin-regulated Glut4 translocation: Membrane protein trafficking with six distinctive steps. *J. Biol. Chem.* **289**, 17280–17298. doi:10.1074/jbc.M114.555714
- Camus, S. M., Camus, M. D., Figueras-Novoa, C., Boncompain, G., Sadacca, L. A., Esk, C., Bigot, A., Gould, G. W., Kioumourtoglou, D., Perez, F., et al. (2020). CHC22 clathrin mediates traffic from early secretory compartments for human GLUT4 pathway biogenesis. *J. Cell Biol.* **219**, e201812135. doi:10.1083/jcb.201812135
- Carlotti, F., Bazuine, M., Kekalainen, T., Seppen, J., Pogoniec, P., Maassen, J. A. and Hoeben, R. C. (2004). Lentiviral vectors efficiently transduce quiescent mature 3T3-L1 adipocytes. *Mol. Ther.* **9**, 209–217. doi:10.1016/j.ythet.2003.11.021
- Caselli, A., Mazzinghi, B., Camici, G., Manao, G. and Ramponi, G. (2002). Some protein tyrosine phosphatases target in part to lipid rafts and interact with caveolin-1. *Biochem. Biophys. Res. Commun.* **296**, 692–697. doi:10.1016/S0006-291X(02)00928-2
- Dascher, C. and Balch, W. E. (1994). Dominant inhibitory mutants of ARF1 block endoplasmic reticulum to Golgi transport and trigger disassembly of the Golgi apparatus. *J. Biol. Chem.* **269**, 1437–1448. doi:10.1016/S0021-9258(17)42277-0
- D'Souza-Schorey, C. and Chavrier, P. (2006). ARF proteins: roles in membrane traffic and beyond. *Nat. Rev. Mol. Cell Biol.* **7**, 347–358. doi:10.1038/nrm1910
- De Lisle, R. C. and Bansal, R. (1996). Brefeldin A inhibits the constitutive-like secretion of a sulfated protein in pancreatic acinar cells. *Eur. J. Cell Biol.* **71**, 62–71.
- Deng, Y., Rivera-Molina, F. E., Toomre, D. K. and Burd, C. G. (2016). Sphingomyelin is sorted at the trans Golgi network into a distinct class of secretory vesicle. *Proc. Natl. Acad. Sci. USA* **113**, 6677–6682.
- Deng, Y., Pakdel, M., Blank, B., Sundberg, E. L., Burd, C. G. and von Blume, J. (2018). Activity of the SPCA1 calcium pump couples sphingomyelin synthesis to sorting of secretory proteins in the Trans-Golgi network. *Dev. Cell* **47**, 464–478.e8. doi:10.1016/j.devcel.2018.10.012
- Egea-Jimenez, A. L. and Zimmermann, P. (2018). Phospholipase D and phosphatidic acid in the biogenesis and cargo loading of extracellular vesicles. *J. Lipid Res.* **59**, 1554–1560. doi:10.1194/jlr.R083964
- Eiseler, T., Wille, C., Koehler, C., Illing, A. and Seufferlein, T. (2016). Protein kinase D2 assembles a multiprotein complex at the trans-Golgi network to regulate matrix metalloproteinase secretion. *J. Biol. Chem.* **291**, 462–477. doi:10.1074/jbc.M115.673582
- Flores-Riveros, J. R., Mclenithan, J. C., Ezaki, O. and Lane, M. D. (1993). Insulin down-regulates expression of the insulin-responsive glucose transporter (GLUT4) gene: Effects on transcription and mRNA turnover. *Proc. Natl. Acad. Sci. USA* **90**, 512–516. doi:10.1073/pnas.90.2.512
- Gao, L., Chen, J., Gao, J., Wang, H. and Xiong, W. (2017). Super-resolution microscopy reveals the insulin-resistance-regulated reorganization of GLUT4 on plasma membranes. *J. Cell Sci.* **130**, 396–405. doi:10.1242/jcs.192450
- Graham, T. R., Scott, P. A. and Emr, S. D. (1993). Brefeldin A reversibly blocks early but not late protein transport steps in the secretory pathway. *EMBO J.* **12**, 869–877. doi:10.1002/j.1460-2075.1993.tb05727.x
- Gunn, K. H., Roberts, B. S., Wang, F., Strauss, J. D., Borgnia, M. J., Egelman, E. H. and Neher, S. B. (2020). The structure of helical lipoprotein lipase reveals an unexpected twist in lipase storage. *Proc. Natl. Acad. Sci. USA* **117**, 10254–10264. doi:10.1073/pnas.1916555117
- Hausser, A., Storz, P., Märten, S., Link, G., Toker, A. and Pfizenmaier, K. (2005). Protein kinase D regulates vesicular transport by phosphorylating and activating phosphatidylinositol-4 kinase III $\beta$  at the Golgi complex. *Nat. Cell Biol.* **7**, 880–886. doi:10.1038/ncb1289
- Hayne, C. K., Lafferty, M. J., Eglinger, B. J., Kane, J. P. and Neher, S. B. (2017). Biochemical analysis of the lipoprotein lipase truncation variant, LPLS447X, reveals increased lipoprotein uptake. *Biochemistry* **56**, 525–533. doi:10.1021/acs.biochem.6b00945
- Hendricks, L. C., McClanahan, S. L., Palade, G. E. and Farquhar, M. G. (1992). Brefeldin A affects early events but does not affect late events along the exocytic pathway in pancreatic acinar cells. *Proc. Natl. Acad. Sci. USA* **89**, 7242–7246. doi:10.1073/pnas.89.15.7242
- Huang, Y., Li, X., Wang, M., Ning, H., Lima, A., Li, Y. and Sun, C. (2013). Lipoprotein lipase links vitamin D, insulin resistance, and type 2 diabetes: a cross-sectional epidemiological study. *Cardiovasc. Diabetol.* **12**, 1–8. doi:10.1186/1475-2840-12-17
- Humphrey, S. J., Yang, G., Yang, P., Fazakerley, D. J., Stöckli, J., Yang, J. Y. and James, D. E. (2013). Dynamic adipocyte phosphoproteome reveals that akt directly regulates mTORC2. *Cell Metab.* **17**, 1009–1020. doi:10.1016/j.cmet.2013.04.010
- Imamura, T., Huang, J., Usui, I., Satoh, H., Bever, J. and Olefsky, J. M. (2003). Insulin-induced GLUT4 translocation involves protein kinase C- $\lambda$ -mediated functional coupling between Rab4 and the motor protein kinesin. *Mol. Cell Biol.* **23**, 4892–4900. doi:10.1128/MCB.23.14.4892-4900.2003
- James, D. E., Brown, R., Navarro, J. and Pilch, P. F. (1988). Insulin-regulatable tissues express a unique insulin-sensitive glucose transport protein. *Nature* **333**, 183–185. doi:10.1038/333183a0
- Jedrychowski, M. P., Gartner, C. A., Gygi, S. P., Zhou, L., Herz, J., Kandror, K. V. and Pilch, P. F. (2010). Proteomic analysis of GLUT4 storage vesicles reveals LRP1 to be an important vesicle component and target of insulin signaling. *J. Biol. Chem.* **285**, 104–114. doi:10.1074/jbc.M109.040428
- Jenkins, G. M. and Frohman, M. A. (2005). Phospholipase D: a lipid centric review. *Cell. Mol. Life Sci.* **62**, 2305–2316. doi:10.1007/s00018-005-5195-z
- Jensen, D. D., Zhao, P., Jimenez-Vargas, N. N., Lieu, T. M., Gerges, M., Yeatman, H. R., Canals, M., Vanner, S. J., Poole, D. P., Bunnett, N. W., et al. (2016). Protein kinase D and G $\beta\gamma$  subunits mediate agonist-evoked translocation of protease-activated receptor-2 from the golgi apparatus to the plasma membrane. *J. Biol. Chem.* **291**, 11285–11299. doi:10.1074/jbc.M115.710681

- Jung, J. J., Tiwari, A., Inamdar, S. M., Thomas, C. P., Goel, A. and Choudhury, A. (2012). Secretion of soluble vascular endothelial growth factor receptor 1 (sVEGFR1/sFlt1) requires Arf1, Arf6, and Rab11 GTPases. *PLoS ONE* **7**, e44572. doi:10.1371/annotation/19ed28f9-9a01-4af9-857d-3ec4aaeacea1
- Kanaha, Y., Nishida, A. and Nozawa, Y. (1992). Calcium rather than protein kinase C is the major factor to activate phospholipase D in FMLP-stimulated rabbit peritoneal neutrophils: possible involvement of calmodulin/myosin L chain kinase pathway. *J. Immunol.* **149**, 622-628.
- Kim, S. J., Nian, C. and McIntosh, C. H. S. (2007). Resistin is a key mediator of glucose-dependent insulinotropic polypeptide (GIP) stimulation of lipoprotein lipase (LPL) activity in adipocytes. *J. Biol. Chem.* **282**, 34139-34147. doi:10.1074/jbc.M704896200
- Kim, M. S., Kewalramani, G., Puthanveetil, P., Lee, V., Kumar, U., An, D., Abrahani, A. and Rodrigues, B. (2008). Acute diabetes moderates trafficking of cardiac lipoprotein lipase through p38 mitogen-activated protein kinase-dependent actin cytoskeleton organization. *Diabetes* **57**, 64-76. doi:10.2337/db07-0832
- Kim, M. S., Wang, F., Puthanveetil, P., Kewalramani, G., Innis, S., Marzban, L., Steinberg, S. F., Webber, T. D., Kieffer, T. J., Abrahani, A., et al. (2009). Cleavage of protein kinase D after acute hypoinsulinemia prevents excessive lipoprotein lipase-mediated cardiac triglyceride accumulation. *Diabetes* **58**, 2464-2475. doi:10.2337/db09-0681
- Klinger, S. C., Glerup, S., Raarup, M. K., Mari, M. C., Nyegaard, M., Koster, G., Prabakaran, T., Nilsson, S. K., Kjaergaard, M. M., Bakke, O., et al. (2011). SorLA regulates the activity of lipoprotein lipase by intracellular trafficking. *J. Cell Sci.* **124**, 1095-1105. doi:10.1242/jcs.072538
- Kraemer, F. B., Takeda, D., Natu, V. and Sztalryd, C. (1998). Insulin regulates lipoprotein lipase activity in rat adipose cells via wortmannin- and rapamycin-sensitive pathways. *Metabolism* **47**, 555-559. doi:10.1016/S0026-0495(98)90239-6
- Kroupa, O., Vorrsoj, E., Stienstra, R., Mattijssen, F., Nilsson, S. K., Sukonina, V., Kersten, S., Olivecrona, G. and Olivecrona, T. (2012). Linking nutritional regulation of Angptl4, Gphbp1, and Lmf1 to lipoprotein lipase activity in rodent adipose tissue. *BMC Physiol.* **12**, 13. doi:10.1186/1472-6793-12-13
- Kumar, M., Ojha, S., Rai, P., Joshi, A., Kamat, S. S. and Mallik, R. (2019). Insulin activates intracellular transport of lipid droplets to release triglycerides from the liver. *J. Cell Biol.* **218**, 3697-3713. doi:10.1083/jcb.201903102
- Kumudu, H., Perera, I., Clarke, M., Morris, N. J., Hong, W., Chamberlain, L. H. and Gould, G. W. (2003). Syntaxin 6 Regulates Glut4 Trafficking in 3T3-L1 Adipocytes. *Mol. Biol. Cell* **14**, 2946-2958. doi:10.1091/mbc.e02-11-0722
- Kupriyanova, T. A., Kandror, V. and Kandror, K. V. (2002). Isolation and characterization of the two major intracellular Glut4 storage compartments. *J. Biol. Chem.* **277**, 9133-9138. doi:10.1074/jbc.M106999200
- Lambert, J. E. and Parks, E. J. (2012). Postprandial metabolism of meal triglyceride in humans. *Biochim. Biophys. Acta Mol. Cell Biol. Lipids* **1821**, 721-726. doi:10.1016/j.bbalip.2012.01.006
- Li, Q., Zhu, X., Ishikura, S., Zhang, D., Gao, J., Sun, Y., Contreras-Ferrat, A., Foley, K. P., Lavandero, S., Yao, Z., et al. (2014). Ca<sup>2+</sup> signals promote GLUT4 exocytosis and reduce its endocytosis in muscle cells. *Am. J. Physiol. Endocrinol. Metab.* **307**, 209-224. doi:10.1152/ajpendo.00045.2014
- Li, L., Beauchamp, M.-C. and Renier, G. (2002). Peroxisome proliferator-activated receptor alpha and gamma agonists upregulate human macrophage lipoprotein lipase expression. *Atherosclerosis* **165**, 101-110. doi:10.1016/S0021-9150(02)00203-4
- Lizunov, V. A., Stenkula, K., Troy, A., Cushman, S. W. and Zimmerberg, J. (2013). Insulin regulates Glut4 confinement in plasma membrane clusters in adipose cells. *PLoS ONE* **8**, e57559. doi:10.1371/journal.pone.0057559
- Martin, S., Millar, C. A. A., Lyttle, C. T. T., Meerloo, T., Marsh, B. J. J., Gould, G. W. W. and James, D. E. E. (2000). Effects of insulin on intracellular GLUT4 vesicles in adipocytes: evidence for a secretory mode of regulation. *J. Cell Sci.* **113**, 3427-3438. doi:10.1242/jcs.113.19.3427
- Miettinen, H. M., Edwards, S. N. and Jalkanen, M. (1994). Analysis of transport and targeting of syndecan-1: Effect of cytoplasmic tail deletions. *Mol. Biol. Cell* **5**, 1325-1339. doi:10.1091/mbc.5.12.1325
- Morrison, D. J., Kowalski, G. M., Grespan, E., Mari, A., Bruce, C. R. and Wadley, G. D. (2018). Measurement of postprandial glucose fluxes in response to acute and chronic endurance exercise in healthy humans. *Am. J. Physiol. Endocrinol. Metab.* **314**, E503-E511. doi:10.1152/ajpendo.00316.2017
- Nakai, W., Kondo, Y., Saitoh, A., Naito, T., Nakayama, K. and Shin, H. W. (2013). ARF1 and ARF4 regulate recycling endosomal morphology and retrograde transport from endosomes to the Golgi apparatus. *Mol. Biol. Cell* **24**, 2570-2581. doi:10.1091/mbc.e13-04-0197
- Nakamura, N., Akashi, T., Taneda, T., Kogo, H., Kikuchi, A. and Fujimoto, T. (2004). ADRP is dissociated from lipid droplets by ARF1-dependent mechanism. *Biochem. Biophys. Res. Commun.* **322**, 957-965. doi:10.1016/j.bbrc.2004.08.010
- Ong, J. M., Kirchgessner, T. G., Schotz, M. C. and Kern, P. A. (1988). Insulin increases the synthetic rate and messenger RNA level of lipoprotein lipase in isolated rat adipocytes. *J. Biol. Chem.* **263**, 12933-12938. doi:10.1016/S0021-9258(88)37651-8
- Park, J., Blanchette-Mackie, E. J. and Scow, R. O. (1996). Brefeldin A enables synthesis of active lipoprotein lipase in cld/cld and castanospermine-treated mouse brown adipocytes via translocation of Golgi components to endoplasmic reticulum. *Biochem. J.* **317**, 125-134. doi:10.1042/bj3170125
- Pradines-Figueroa, A., Vannier, C. and Ailhaud, G. (1990). Lipoprotein lipase stored in adipocytes and muscle cells is a cryptic enzyme. *J. Lipid Res.* **31**, 1467-1476. doi:10.1016/S0022-2275(20)42617-3
- Pusapati, G. V., Krndija, D., Armacki, M., von Wichert, G., von Blume, J., Malhotra, V., Adler, G. and Seufferlein, T. (2009). Role of the second cysteine-rich domain and Pro275 in protein kinase D2 interaction with ADP-ribosylation factor 1, trans-Golgi network recruitment, and protein transport. *Mol. Biol. Cell* **21**, 845-1152. doi:10.1091/mbc.e09-09-0814
- Reizes, O., Goldberger, O., Smith, A. C., Xu, Z., Bernfield, M. and Bickel, P. E. (2006). Insulin promotes shedding of syndecan ectodomains from 3T3-L1 adipocytes: a proposed mechanism for stabilization of extracellular lipoprotein lipase. *Biochemistry* **45**, 5703-5711. doi:10.1021/bi052263h
- Roberts, B. S., Babilonia-Rosa, M. A., Broadwell, L. J., Wu, M. J. and Neher, S. B. (2018). Lipase maturation factor 1 affects redox homeostasis in the endoplasmic reticulum. *EMBO J.* **37**, e97379. doi:10.15252/embj.201797379
- Roh, C., Roduit, R., Thorens, B., Fried, S. and Kandror, K. V. (2001). Lipoprotein lipase and leptin are accumulated in different secretory compartments in rat adipocytes. *J. Biol. Chem.* **276**, 35990-35994. doi:10.1074/jbc.M102791200
- Rossi, G., Watson, K., Kennedy, W. and Brennwald, P. (2018). The tomosyn homologue, Sro7, is a direct effector of the Rab GTPase, Sec4, in post-Golgi vesicle tethering. *Mol. Biol. Cell* **29**, 1476-1486. doi:10.1091/mbc.E18-02-0138
- Ruby, M. A., Goldenson, B., Orasanu, G., Johnston, T. P., Plutsky, J. and Krauss, R. M. (2010). VLDL hydrolysis by LPL activates PPAR- $\alpha$  through generation of unbound fatty acids. *J. Lipid Res.* **51**, 2275-2281. doi:10.1194/jlr.M005561
- Sadler, J. B. A., Lamb, C. A., Gould, G. W. and Bryant, N. J. (2016). Complete membrane fractionation of 3T3-L1 adipocytes. *Cold Spring Harb. Protocols* **2016**, 193-198. doi:10.1101/pdb.prot083691
- Saltiel, A. R. and Kahn, C. R. (2001). Insulin signalling and the regulation of glucose and lipid metabolism. *Nature* **414**, 799-806. doi:10.1038/414799a
- Sano, H., Eguez, L., Teruel, M. N., Fukuda, M., Chuang, T. D., Chavez, J. A., Lienhard, G. E. and McGraw, T. E. (2007). Rab10, a target of the AS160 Rab GAP, is required for insulin-stimulated translocation of GLUT4 to the adipocyte plasma membrane. *Cell Metab.* **5**, 293-303. doi:10.1016/j.cmet.2007.03.001
- Schindelin, J., Arganda-Carreras, I., Frise, E., Kaynig, V., Longair, M., Pietzsch, T., Preibisch, S., Rueden, C., Saalfeld, S., Schmid, B., et al. (2012). Fiji: An open-source platform for biological-image analysis. *Nat. Methods* **9**, 676-682. doi:10.1038/nmeth.2019
- Schoonjans, K., Peinado-Onsurbe, J., Lefebvre, A. M., Heyman, R. A., Briggs, M., Deeb, S., Staels, B. and Auwerx, J. (1996). PPAR $\alpha$  and PPAR $\gamma$  activators direct a distinct tissue-specific transcriptional response via a PPRE in the lipoprotein lipase gene. *EMBO J.* **15**, 5336-5348. doi:10.1002/j.1460-2075.1996.tb00918.x
- Semenkovich, C. F., Wims, M., Noe, L., Etienne, J. and Chan, L. (1989). Insulin regulation of lipoprotein lipase activity in 3T3-L1 adipocytes is mediated at posttranscriptional and posttranslational levels. *J. Biol. Chem.* **264**, 9030-9038. doi:10.1016/S0021-9258(88)81898-1
- Semenkovich, C. F., Chen, S. H., Wims, M., Luo, C. C., Li, W. H. and Chan, L. (1989b). Lipoprotein lipase and hepatic lipase mRNA tissue specific expression, developmental regulation, and evolution. *J. Lipid Res.* **30**, 423-431. doi:10.1016/S0022-2275(20)38369-3
- Shome, K., Vasudevan, C. and Romero, G. (1997). ARF proteins mediate insulin-dependent activation of phospholipase D. *Curr. Biol.* **7**, 387-396. doi:10.1016/S0960-9822(06)00186-2
- Simsolo, R. B., Ong, J. M. and Kern, P. A. (1992). Characterization of lipoprotein lipase activity, secretion, and degradation at different sites of post-translational processing in primary cultures of rat adipocytes. *J. Lipid Res.* **33**, 1777-1784. doi:10.1016/S0022-2275(20)41335-5
- Slot, J. W., Garruti, G., Martin, S., Oorschot, V., Posthuma, G., Kraegen, E. W., Laybutt, R., Thibault, G. and James, D. E. (1997). Glucose transporter (GLUT-4) is targeted to secretory granules in rat atrial cardiomyocytes. *J. Cell Biol.* **137**, 1243-1254. doi:10.1083/jcb.137.6.1243
- Stalder, D. and Gershlick, D. C. (2020). Direct trafficking pathways from the Golgi apparatus to the plasma membrane. *Semin. Cell Dev. Biol.* **107**, 112-125. doi:10.1016/j.semcdb.2020.04.001
- Stenkula, K. G., Lizunov, V. A., Cushman, S. W. and Zimmerberg, J. (2010). Insulin controls the spatial distribution of GLUT4 on the cell surface through regulation of its postfusion dispersal. *Cell Metab.* **12**, 250-259. doi:10.1016/j.cmet.2010.08.005
- Sundberg, E. L., Deng, Y. and Burd, C. G. (2019). Syndecan-1 Mediates Sorting of Soluble Lipoprotein Lipase with Sphingomyelin-Rich Membrane in the Golgi Apparatus. *Dev. Cell* **51**, 387-398.e4. doi:10.1016/j.devcel.2019.08.014
- Tie, H. C., Ludwig, A., Sandin, S. and Lu, L. (2018). The spatial separation of processing and transport functions to the interior and periphery of the golgi stack. *Elife* **7**, 1-26. doi:10.7554/eLife.41301

- Vannier, C., Deslex, S., Pradines-Figueres, A. and Ailhaud, G. (1989). Biosynthesis of lipoprotein lipase in cultured mouse adipocytes. I. Characterization of a specific antibody and relationships between the intracellular and secreted pools of the enzyme. *J. Biol. Chem.* **264**, 13199-13205. doi:10.1016/S0021-9258(18)51615-X
- Wang, P., Mariman, E., Keijer, J., Bouwman, F., Noben, J. P., Robben, J. and Renes, J. (2004). Profiling of the secreted proteins during 3T3-L1 adipocyte differentiation leads to the identification of novel adipokines. *Cell. Mol. Life Sci.* **61**, 2405-2417. doi:10.1007/s00018-004-4256-z
- Wang, P., Keijer, J., Bunschoten, A., Bouwman, F., Renes, J. and Mariman, E. (2006). Insulin modulates the secretion of proteins from mature 3T3-L1 adipocytes: A role for transcriptional regulation of processing. *Diabetologia* **49**, 2453-2462. doi:10.1007/s00125-006-0321-5
- Wang, Y., Ali, Y., Lim, C.-Y., Hong, W., Pang, Z. P. and Han, W. (2014). Insulin-stimulated leptin secretion requires calcium and PI3K/Akt activation. *Biochem. J.* **458**, 491-498. doi:10.1042/BJ20131176
- Worrall, D. S. and Olefsky, J. M. (2002). The effects of intracellular calcium depletion on insulin signaling in 3T3-L1 adipocytes. *Mol. Endocrinol.* **16**, 378-389. doi:10.1210/mend.16.2.0776
- Xiao, Y., Wang, C., Chen, J. Y., Lu, F., Wang, J., Hou, N., Hu, X., Zeng, F., Ma, D., Sun, X., et al. (2018). Deficiency of PRKD2 triggers hyperinsulinemia and metabolic disorders. *Nat. Commun.* **9**, 1-11. doi:10.1038/s41467-017-02088-w
- Xie, L., O'Reilly, C. P., Chapes, S. K. and Mora, S. (2008). Adiponectin and leptin are secreted through distinct trafficking pathways in adipocytes. *Biochim. Biophys. Acta* **1782**, 99-108. doi:10.1016/j.bbadis.2007.12.003
- Xie, B., Chen, Q., Chen, L., Sheng, Y., Wang, H. Y. and Chen, S. (2016). The inactivation of RabGAP function of AS160 promotes lysosomal degradation of GLUT4 and causes postprandial hyperglycemia and hyperinsulinemia. *Diabetes* **65**, 3327-3340. doi:10.2337/db16-0416
- Xu, H. and Ren, D. (2015). Lysosomal physiology. *Annu. Rev. Physiol.* **77**, 57-80. doi:10.1146/annurev-physiol-021014-071649
- Yang, C. Z. and Mueckler, M. (1999). ADP-ribosylation factor 6 (ARF6) defines two insulin-regulated secretory pathways in adipocytes. *J. Biol. Chem.* **274**, 25297-25300. doi:10.1074/jbc.274.36.25297
- Yeh, T.-Y. J., Sbodio, J. I., Tsun, Z.-Y., Luo, B. and Chi, N.-W. (2007). Insulin-stimulated exocytosis of GLUT4 is enhanced by IRAP and its partner tankyrase. *Biochem. J.* **402**, 279-290. doi:10.1042/BJ20060793



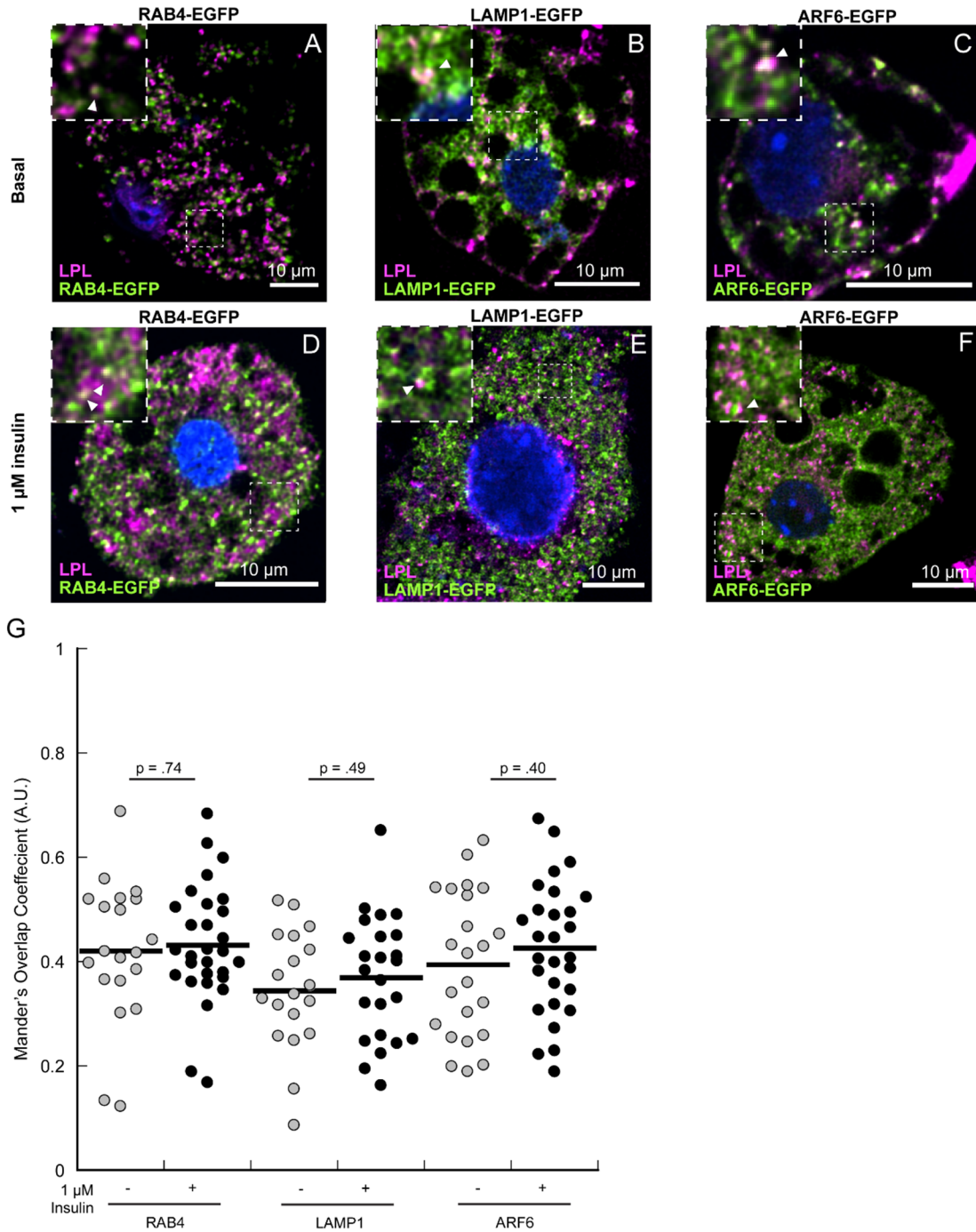


**Fig. S1. LPL colocalization with RAB4, LAMP1, and ARF6**

A-C) Adipocytes were treated with vehicle (basal) or (D-F) with insulin for 120 minutes before being fixed and stained for the indicated target. Insets show selected zoomed-in views. Scale bars = 10  $\mu\text{m}$ . Examples of colocalizing puncta are indicated with arrows. G) The colocalization of LPL with the indicated markers by the Mander's coefficient is shown. All datasets include 3 biological replicate sets: RAB4 (basal n=20; IS n=29), LAMP1 (basal n=19; IS n=24), ARF6 (basal n=23; IS n=28). P-values were calculated with a Student's t-test.

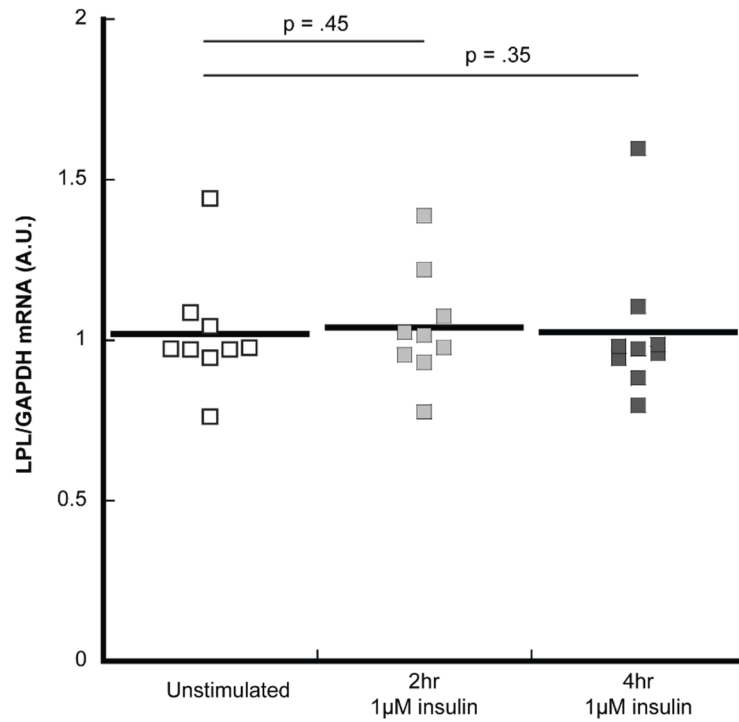


**Fig. S2. Acute insulin treatment does not affect LPL mRNA levels**

mRNA was collected from cells grown under cell culture conditions and RT-qPCR was used to measure LPL mRNA relative to GAPDH mRNA. Each point represents a technical replicate. All experiments completed in triplicate. P-values were calculated with a one-way ANOVA with Dunnet's post-hoc test.

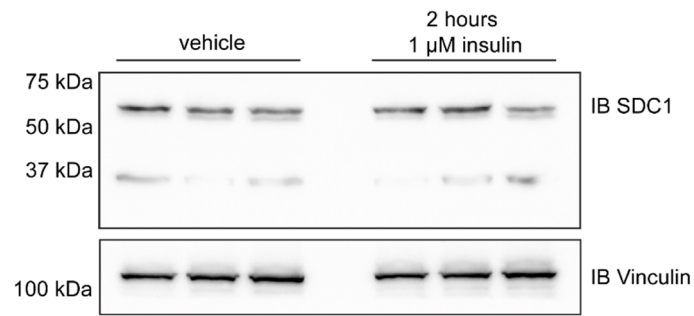


**Fig. S3. Acute insulin treatment does not affect SDC1 levels**

Differentiated 3T3-L1 adipocytes were treated with either vehicle or insulin for 2 hours. Cell lysates were analyzed by Western blot and blotted for SDC1 and vinculin. Samples were collected and analyzed in triplicate.

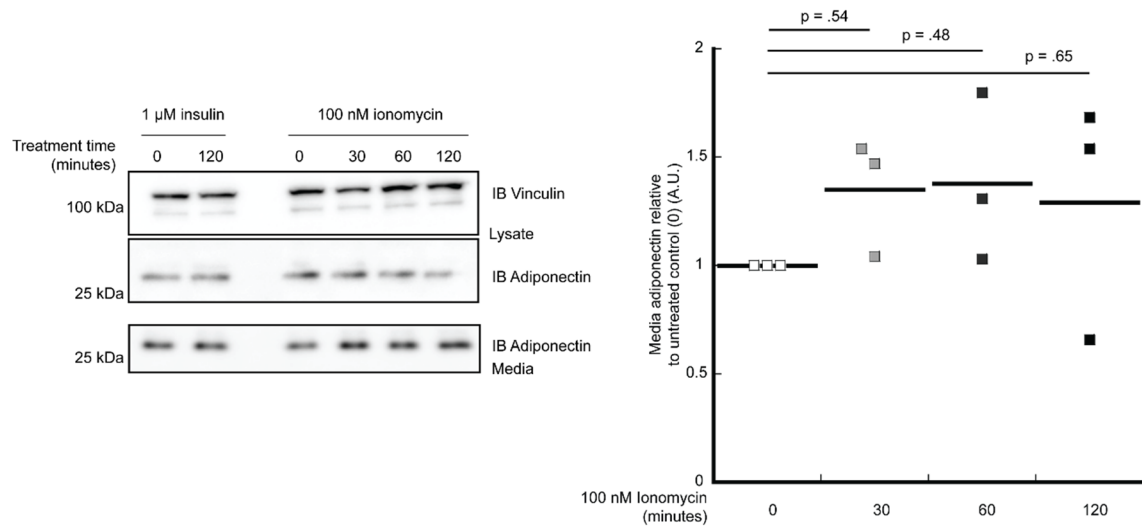


**Fig. S4. Ionomycin treatment does not significantly increase adiponectin secretion**

Cells were treated with either insulin (left) or ionomycin (right) for the indicated times. Untreated cells (0) were treated with vehicle alone. Media adiponectin was measured and plotted relative to untreated cells (0). P-values were calculated by one-way ANOVA with Dunnett's post-hoc test.

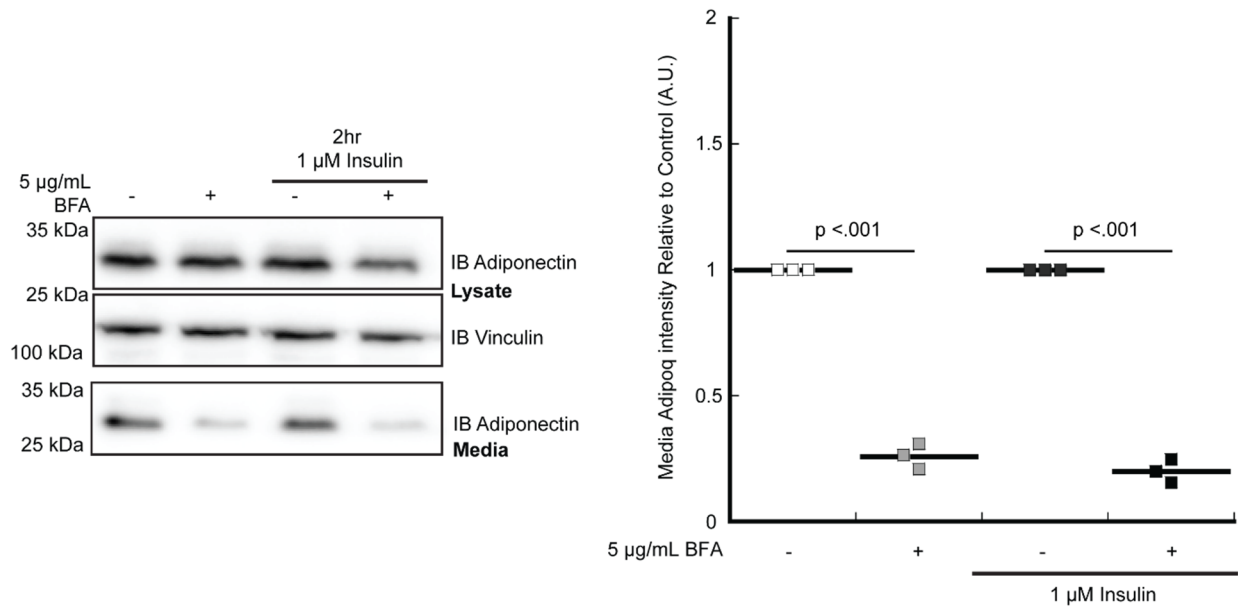


**Fig. S5. BFA partly prevents adiponectin secretion**

Differentiated 3T3-L1 adipocytes were treated with either vehicle, 1 µM insulin, 5 µg/mL BFA, or a combination of insulin and BFA. Cells were pre-treated with BFA or vehicle for 30 minutes before insulin or vehicle was added for 2 hours. Media and lysates were collected after 2 hours and samples were prepared for analysis by Western blot. Samples were blotted for adiponectin and vinculin. Graphs show media adiponectin levels relative to untreated controls for 3 replicate experiments. P-values were calculated with two-way ANOVA with Šidák-corrected pairwise tests. Media adiponectin levels: +BFA / -BFA = 26%±5; IS +BFA / -BFA = 20%±5.

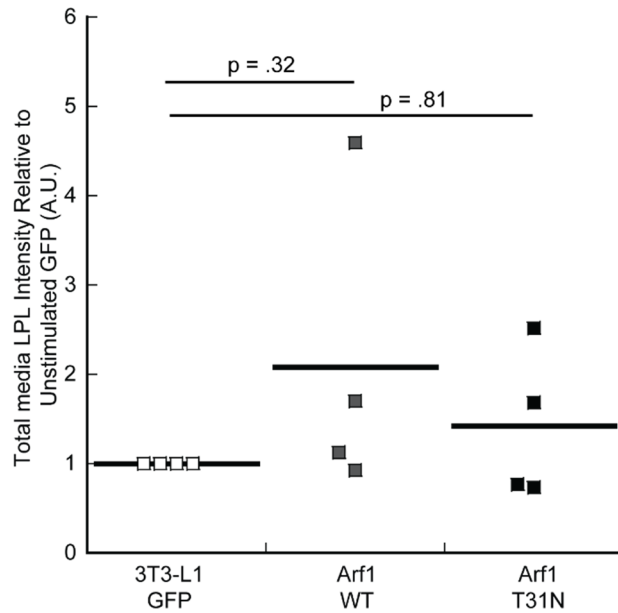


**Fig. S6. LPL secretion relative to unstimulated controls**

Data from Figure 7B was analyzed to show indicate LPL secretion relative to unstimulated GFP controls. There is no difference in LPL secretion from unstimulated cells expressing GFP, ARF1 WT-GFP, and ARF1 T31N-GFP. Full-length LPL band intensity relative to unstimulated cells for 4 replicate experiments are shown. P-values were calculated with a one-way ANOVA with Dunnett's post-hoc test.

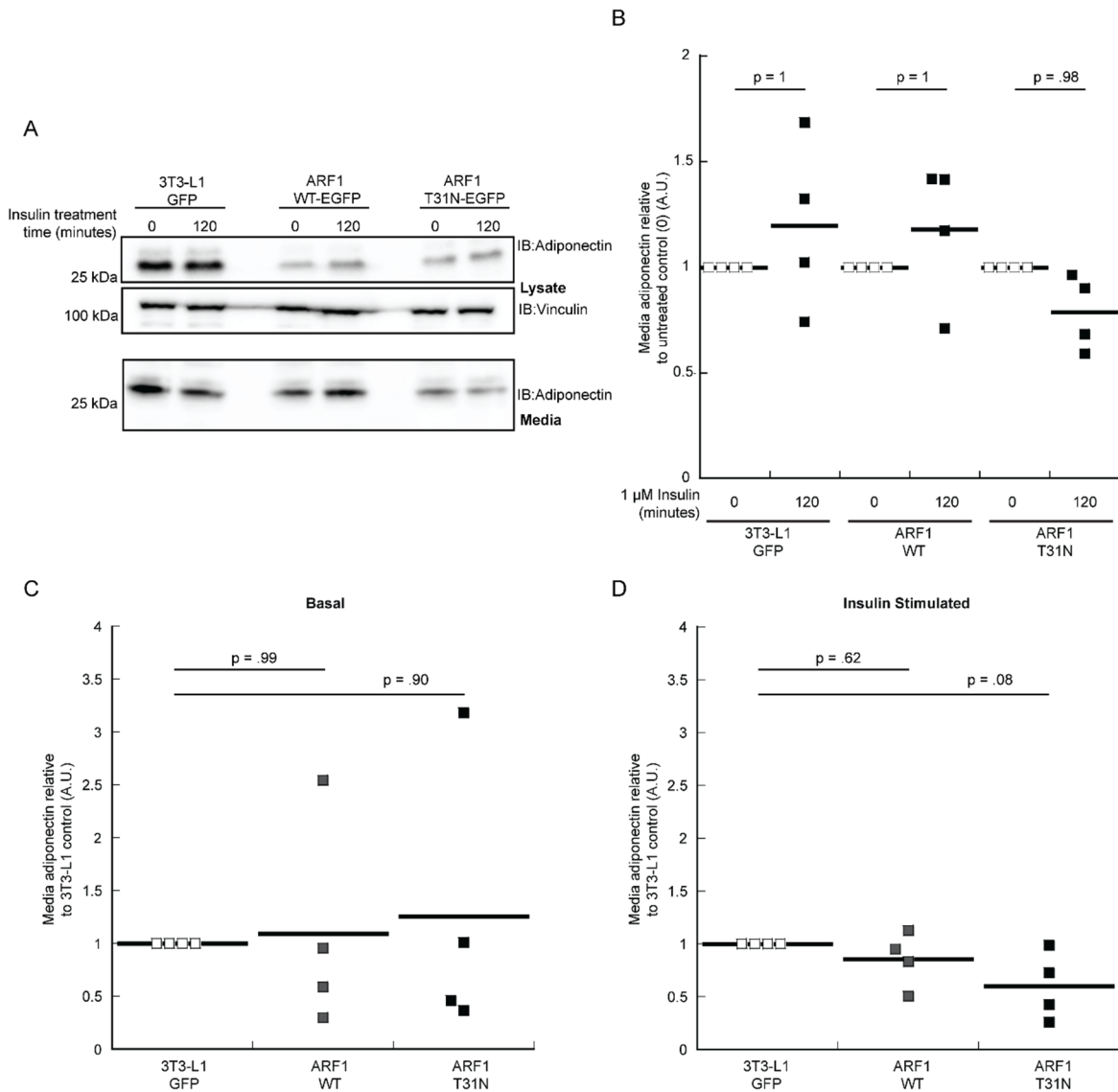


**Fig. S7. ARF1 overexpression does not affect adiponectin secretion**

A) 3T3-L1 adipocytes expressing either GFP, ARF1-WT, or ARF1-T31N were treated with vehicle or 1 $\mu$ M insulin for the indicated times. Media and lysates were collected and samples were analyzed for Adiponectin and vinculin by Western blot. B) Media adiponectin levels are plotted relative to untreated controls. Significant interactions were calculated with a two-way ANOVA and p-values were calculated with Šidák-corrected pairwise tests. C) Media adiponectin levels from unstimulated (basal, 0 minutes) or D) insulin-stimulated cells (120 minutes) are plotted relative to 3T3-GFP control cells. P-values were calculated with a one-way ANOVA with Dunnett's post-hoc test. Results from 4 replicate experiments are shown.